Lipid-membrane interactions of the bovine eye lens

RUTH BARBARA MCTIERNAN

MATERIAL ABSTRACT: LIPID-MEMBRANE INTERACTIONS OF THE BOVINE EYE LENS - RUTH BARBARA MCTIERNAN

The lens is a transparent, biconvex structure within the eye that has a very high refractive index. It focuses light onto the retina and enables vision. It is able to elastically deform to adjust the focal length of the eye for observing objects at varying distances, a process known as accommodation.

With age or damage, the lens becomes stiffer and more likely to develop opaque regions called cataracts. Levels of oxidised lipids such as 7-ketocholesterol increase with age and raised levels of these oxysterols are observed in cataractous lenses.

The goal of this project is to investigate the effect of raised levels of 7-ketocholesterol on the biophysical properties of lens membranes, which could in turn affect the structure of lens fibre cells and thereby impact on their individual function and the lens structure as a whole.

Nanomechanical measurements of the lens elasticity with Atomic Force Microscopy (AFM) show that the Young's Modulus of model and extracted bovine lens lipid membranes are lower when incubated with biologically-relevant levels of 7-ketocholesterol, signalling decreased membrane stiffness. In addition to this, the force required to extract individual thiol-tagged cholesterols from the model membranes was observed to decrease with the presence of 7-ketocholesterol, indicating this is consistent with Fluorescence Recovery After Photobleaching observations of model membranes which support a more fluid membrane with 7-ketocholesterol present as the diffusion coefficient (recovery rate of the membrane) is higher.

Taken together, these findings show how the biophysical properties of the lipid membranes are altered by the presence of 7-ketocholesterol and provide insight for further investigations to examine how the eye lens is affected with age or oxidative damage. A novel model membrane for the lipids of the bovine eye lens was also created and tested, which could be used in further experiments.

Lipid-membrane interactions of the bovine eye lens

Effects of raised levels of 7-ketocholesterol on the biophysical properties of model and native lens membranes

Ruth Barbara McTiernan

Master of Sciences

Biosciences and Physics Departments

Durham University

2018/19

Chapter 1 Table of Contents

List of Tables

List of Illustrations

List of Abbreviations

Abbreviation	Full Term	First appearance
AFM	Atomic Force Microscopy	1
BLAST	Basic Local Alignment Search Tool	38
CBD	Cholesterol bilayer domains	21
CCD	Charge coupled device	39
ECM	Extracellular Matrix	17
EPSL	Electron Paramagnetic Spin-Labelling	21
FRAP	Fluorescence Recovery After Photobleaching	12
FTIR	Fourier Transform Infrared	19
GPMV	Giant Plasma Membrane Vesicles	43
GUV	Giant Unilamellar Vesicles	42
IN	Inner Nucleus	19
L_D	Liquid disordered	16
LFC	Lens fibre cells	10
L_O	Liquid ordered	16
LSS	Lanosterol synthase	69
MALDI	Matrix Assisted Laser Desorption/Ionization	23
MALDI-TOF	Matrix-Assisted Laser Desorption/Ionization-Time Of Flight	23
MLB	Multi lamellar bodies	35
NMR	Nuclear magnetic resonance	19
OC	Outer Cortex	14
PALM	Photo activated localization microscopy	41
PTM	Post-Translational Modification	32
SIM	Structured illumination microscopy	41slm
SLB	Supported Lipid Bilayers	43
SNAP	Standardized Nanomechanical Atomic Force Microscopy Procedure	63
STORM	Stochastic optical reconstruction microscopy	41
SUV	Small Unilamellar Vesicles	43
TEM	Transmission electron microscopy	21
TIRFM	Total Internal Reflection Fluorescence Microscopy	41
VDW	Van der Waal	18
YM	Young's Modulus	12

Statement of Copyright

Acknowledgements

I would like to thank my supervisors, Prof Quinlan and Dr Voïtchovsky, for all their support and guidance over the course of the year. They have enabled me to pursue my research interests across departmental boundaries.

Dedication

To Veronique Peacock; without your support I highly doubt I would have completed my undergraduate degree, let alone this Masters – I cannot thank you enough, but this is a start.

Chapter 1 Introduction

The aim of this research is to observe how the biophysical properties of eye lens membranes are affected by the inclusion of the oxysterol 7-ketocholesterol, which is known to accumulate in membranes of the eye lens as it ages and is found in raised levels in cataractous lenses. This will give insight into how changes to the lens lipidome with age contribute to the large-scale lens defects found in cataract and presbyopia; the clouding and stiffening of the lens tissue, respectively.

To understand the multi-scale changes to the lens with age and disease, an overview is needed of healthy lens structure and function across the scales of the lipidome, full membrane, cell, multi-cell and whole tissue. From there comparison with known changes in ageing and disease are made. Methodologies for studying biomechanics of the lens on different scales are addressed and known properties related to this thesis introduced.

1.1.1 The Eye Lens

The sense of sight is one of, if not the most important of the senses for many animals; a view of the world around is vital to everything from identifying danger, to navigating terrain and hunting prey.

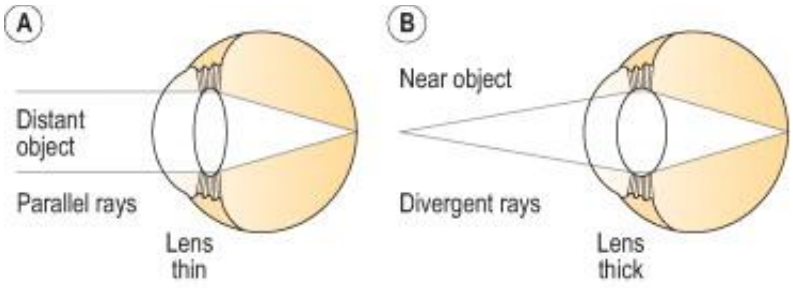

Figure 1: The process of lens accommodation in mammals helps to focus light onto the retina at the back of the eye by altering the shape of the lens. In a young, healthy lens objects from approximately 6.5 cm away to infinity cam be brought into sharp focus. a) Focusing on distant objects occurs by contraction of the zonule fibres to thin the lens. b) Focusing on close objects is achieved by relaxation of the zonule fibres, releasing the stretch on the lens and allowing it to thicken. Taken from the paper by Michael-Titus [1].

The lens is positioned behind the iris within the eye, between the clear fluid aqueous and vitreous humors. It is suspended by ligaments called zonule fibres that are attached to the anterior ciliary body [2]. In mammals, reptiles and birds, these zonule fibres can contract and relax to elastically deform the lens, shifting the focal length of the eye in a process called accommodation (Figure 1). This allows objects at different distances to be brought into sharp focus. Amphibians and fish achieve this by moving the whole lens backwards and forwards

within the eye [3]. The lens must also be transparent to allow light to pass through it, and diffract light to focus it onto the retina.

To perform these functions the lens is made up of highly specialised, tightly organised cells – the bulk of which are lens fibre cells (LFCs).

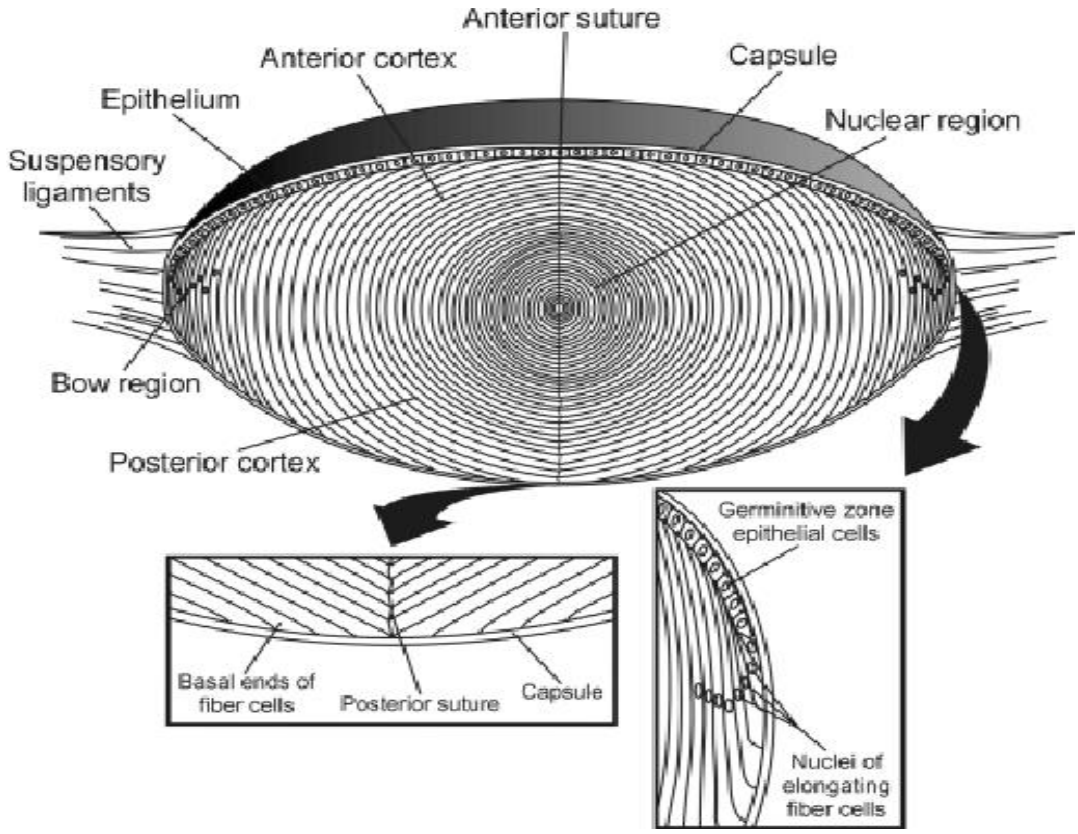

Figure 2: Lens cell arrangement. The bulk of cells in the lens are fibre cells, which grow inwards from the germinitive zone at the bow region of the lens equator in successive layers, elongating and losing most organelles to become transparent and meeting along the central suture line. Image taken from the paper by Beebe [4].

Once terminally differentiated, they lose most of their organelles (which would normally block incident light), have membranes containing the highest cholesterol content in the body [5], and are packed with crystallin proteins. They grow inwards from the equator in layers (Figure 2) that resemble a honeycomb structure when cross-sectioned and have a very low turnover rate, with individual LFCs lasting on the order of decades despite regular exposure to ultraviolet (UV) light.

Changes to the lens occur with increasing age; older lenses become stiffer and less transparent, and the lipid content changes. Proteins present in the lens accumulate modifications over time and may begin to function less effectively, or form aggregates that can disrupt light transmission.

1.1.2 Cataract

Cataracts are a degeneration of the eye lens characterised by clouding, causing distortion and blocking of incident light and progressively impairing vision. They can take many forms, and are type classified by where they appear in the lens, their size and the degree to which transparency has been lost in the affected region [6]. Most frequently they appear associated with age-related degeneration, but can also be a result of other factors including ocular trauma, radiation exposure, genetic factors or metabolic disorder.

Changes to the lens lipidome occur progressively with age; Relative amounts of dihydro/sphingomyelin and cholesterol increase compared to glycerolipids such as phosphatidylcholine., and levels of oxidised sterols present in the LFC membranes increase, with the most prevalent being 7-ketocholesterol. Oxysterols have been observed to accumulate in cataracts [7], but exactly how the lens membranes are affected by this is not fully understood. A greater understanding of changes to lipid mechanics in cataractous lenses could provide insight into how cell function as a whole is compromised.

Cataracts are responsible for 51% of blindness worldwide and can currently only be treated successfully by surgical removal and lens replacement. In areas with less easy access to treatment or lower income, visual impairment and blindness caused by cataract can go untreated, leaving people dependant on family members for support [8]. The likelihood of cataracts developing increases with age and accumulation of damage in the lens; as populations age the number of people developing age-related cataracts is expected to rise.

Understanding of the mechanisms of cataract formation is therefore increasingly important; preventing the formation and spread of new cataracts, as well as treatment of existing cataracts without the need for surgery would be highly beneficial. This would make treatment accessible to people in areas without readily-available eye care, as well as reducing the rising demand for surgery and making for a healthier, happier old age for people overall.

1.1.3 Presbyopia

Another age-associated disorder of the eye is Presbyopia, which is a decrease in the lens' ability to accommodate (focus on objects close to the eye). It is a common condition to develop with age, as the eye lens stiffens and the eye has more difficulty in focusing light onto the retina – the loss of accommodation power varies, but some degree is inevitable [9]. Whilst not as damaging to vision overall as cataract, understanding the processes involved in this change would help to form a greater understanding of how the lens ages overall.

1.2 Aims

The aim of this work is to observe changes in the biophysical properties of lipid bilayer membranes extracted from or mimicking the composition of the bovine eye lens, when the oxysterol 7-ketocholesterol is incorporated at a biologically-relevant concentration (that observed in cataractous lenses).

Observations are made of membrane fluidity using FRAP, topography and phase are examined using tapping-mode AFM, Young's Modulus (YM) using contact mode AFM and the force required to extract thiol-tagged cholesterol from lipid membranes using AFM with a UV-treated cantilever.

Significant changes at the lipid level will indicate how the function of the cataractous lens is initially compromised and will lay the groundwork for investigations at higher levels of complexity, such as changes to protein-membrane interactions in ageing or cataractous lenses.

Chapter 2 Literature Review

The eye lens' transparency is not solely dependent on composition of the lipidome; the structure and organisation of cells within the lens, their membranes and associated proteins are all important to the function of the organ – To understand how the inclusion of oxysterols such as 7-ketocholesterol into lens cell membranes may give rise to cataract or other lens disorders a view of the whole is important from the outset.

2.1 Cell Structure and Organisation in the Lens

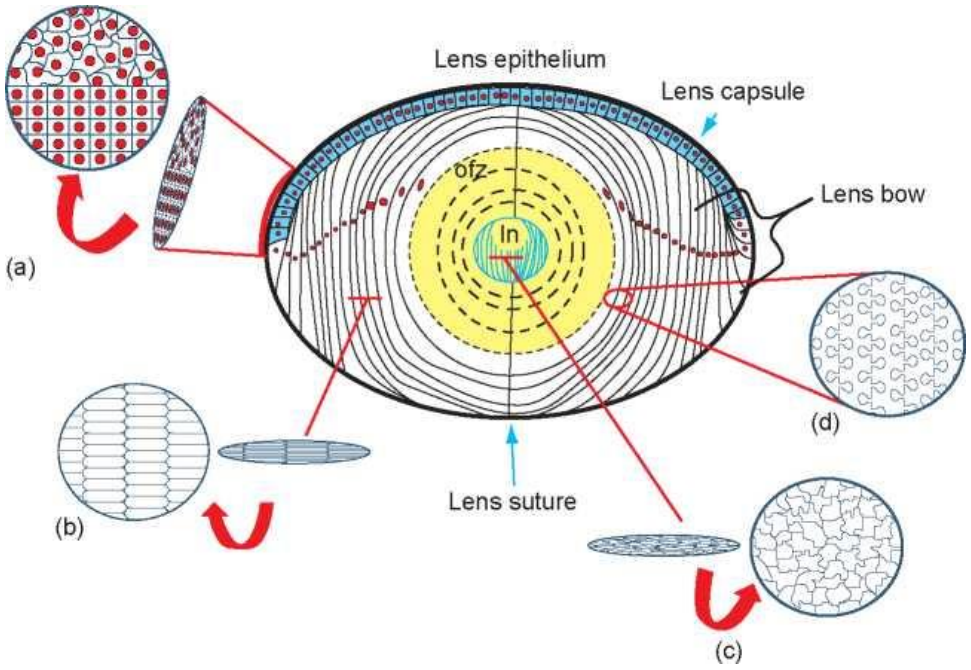

Figure 3: Lens organisation diagram , taken from Aibolita.com[9]: (a) Germinative zone of Lens bow region, where cells are undifferentiated and still contain nuclei, (b) Hexagonal packing of cortical LFCs is evident if cut across the equator, (c) Loss of packing structure occurs in the nuclear region over time, (d) Interlocking cell membrane structure of adjacent LFCs when cut transverse to the equator.

Within the lens capsule cells are organised into two distinct subgroups; Covering the anterior surface is a single layer of epithelial cells, the cells of which are nucleated and carry out most of the active metabolic, synthetic and transport functions of the lens [10]. Below this layer, the bulk of the lens is made up of Lens Fibre Cells (LFCs). The organisation of these cells is tightly controlled; they are packed into concentric shells around the embryonic nucleus. To minimise light scatter, once terminally differentiated Lens Fibre Cells (LFCs) do not contain opaque organelles such as nuclei [11], endoplasmic reticula and mitochondria. These structures are progressively lost as epithelial cells differentiate in from the equatorial regions of the lens, elongating (reaching up to 1cm long) to arc around and converge at the poles

(Figure 3 a-c). This additive process occurs both during development and throughout life, and by this process LFCs are arranged in regularly-ordered, closed sheets.

LFCs undergo extensive membrane remodelling as they differentiate. They lose their nuclei and develop interlocking cell membrane structures with their neighbours (Figure 3 d) to assist with maintaining structural order and stability [12], visible as 'ball and socket' (or 'tongue and groove') structural arrangements when viewed with SEM [13]. The majority of these interdigitations are associated with gap junctions and pores, with the exception of protrusions at cell corners, and they are maintained once formed through to the centre of the lens.

Fibre cells of the Outer Cortex (OC) have hexagonal cross-sections if cut across the equator. (Figure 4) This gives overall a tightly-packed honeycomb structure, which acts as an organic diffraction grating, constructively interfering with light passing straight through and destructively with light travelling in other directions.

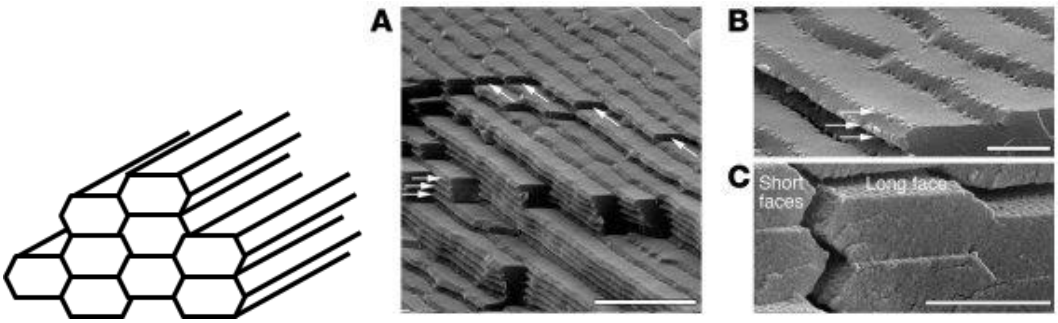

Figure 4: LFC structural arrangement cut across the equator takes the form of a tightly-packed honeycomb lattice. This can be clearly viewed by SEM (a-c), where organised layers of flattened, elongated hexagonal cells are apparent, with membrane protrusions visible at the apex of each short face (b) SEM images taken from the paper by Song [14]**.**

The refractive indices of cytosol and lens cell membranes are closely matched in individual and neighbouring cells by cellular fusions allowing protein exchange – these refractive indices are significantly higher than the surrounding medium to allow the lens to focus light travelling through it, which passes through thousands of cell membranes. The junctional gaps between cells are also kept very tight, well below the wavelength of visible light. The membranes of LFCs match the refractive index of the cytosol progressively more closely as they approach the nucleus – they contain a very high ratio of cholesterol to phospholipid, ranging from 2.2 +/- 0.3 in the outer cortex to 9.2 +/- 1.6 in the nucleus [15].

The high refractive index is achieved in the cytosol by having a very high density of crystallin proteins (sometimes in excess of 450mg/ml) – contrary to the standard expectation of more light scatter occurring with more protein present, at very high concentration, short-range

interactions between the proteins produce destructive interference that practically eliminates light scatter [16].

As blood vessels would interfere with transparency the lens is avascular, so homeostasis inside the lens is maintained by an internal osmotically driven fluid circulation (Figure 5), generated by ion pumps in cells at the equator edge [17]. The LFC membranes and their associated proteins are crucial to this process, and disruption to the system on any level can give rise to significant lens defects.

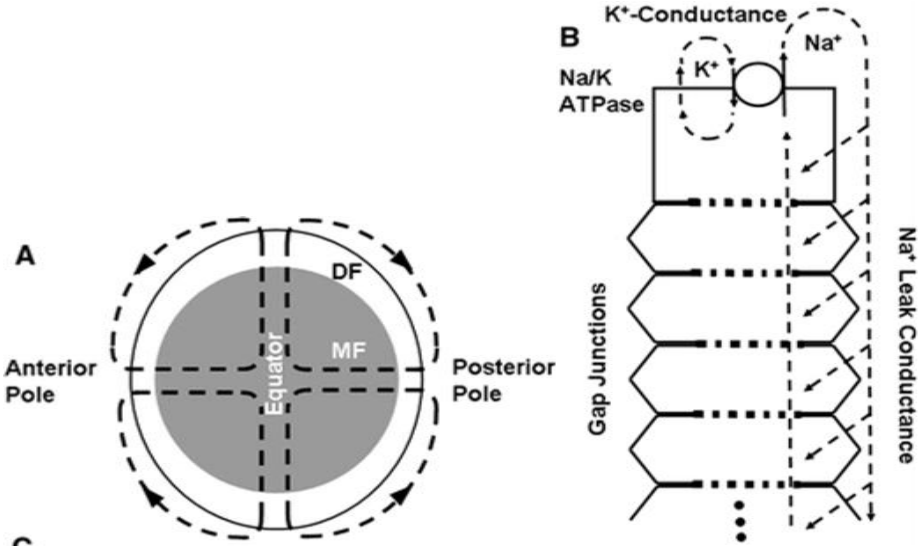

Figure 5: Fluid Circulation in the lens. a) Flow of fluid passes into the lens at the poles and into the centre, eventually being pushed out at the equator edge to recirculate. b) An osmotic gradient is generated by a system of sodium and potassium ion pumps in cells at the equator edge to maintain fluid flow through the lens. Image is adapted from the paper by Mathias [17].

2.2 Cell Membranes

The plasma membrane of a cell forms a barrier between the interior of a cell and the external environment; it allows for control of what moves in and out of the cell, is where external signals can be received to trigger specific responses and provides a highly versatile structural envelope.

Composed primarily of heterogeneously-arranged phospholipids, sphingolipids and cholesterol in an amphipathic lipid bilayer, and containing a high density of proteins and carbohydrates, cell membranes are highly dynamic, complex structures but also tightly regulated. In vivo, cell membranes are found in tightly packed liquid ordered (L_O) and more fluid liquid disordered (L_D) phases dependant on their lipid and protein composition – more saturated, tight-packing lipids are more likely to form L_O phases. This varies between cell types and across individual cells spatially and temporally. Interactions between protein and

membrane are vital to a variety of processes such as membrane trafficking, cell-cell communication, control of membrane fluidity and changing of membrane shape to form protrusions (including filopodia and lamellipodia).

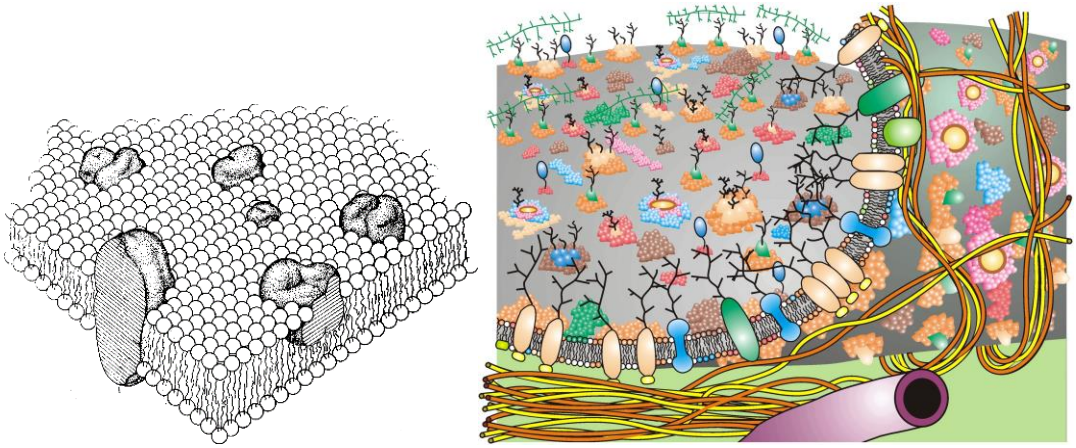

Figure 6: Models of biological membrane structure. Left: The Singer-Nicholson fluid mosaic model, taken from the 1972 paper, depicts the cell membrane as a fluid bilayer of phospholipids with embedded membrane proteins 'floating' through the structure [18]. Right: An updated model image, taken from the paper by Nicolson – newer membrane models are more complex, including membrane domain structures, lipid rafts and membrane-associated extracellular matrix and cytoskeletal elements [19].

Membrane structure can be described through the fluid mosaic model, initially proposed in 1972 and based on thermodynamic principles of membrane lipid organisation, as well as evidence of lateral mobility and asymmetry within the membrane (Figure 6 a) [18]. The fluid mosaic model is still relevant 40 years later, but later work has expanded on the complexity of structure, regulation and dynamics within cell membranes. These aspects include specialised membrane domains, lipid rafts and membrane associations with cytoskeleton and extracellular matrix (ECM) structures. (Figure 6 b) [19]

2.2.1 Eye Lens Membrane

The lipid content of the human eye lens is unusual, compared to both other tissues in the body and the eye lenses of other species. The membranes of LFCs have a high degree of lipid order/saturation, and most lens lipids have their mobility further reduced by association with proteins (Figure 7). Very high levels of Cholesterol allow for lateral segregation of lipids into raft domains and pure cholesterol bilayer patches [20]

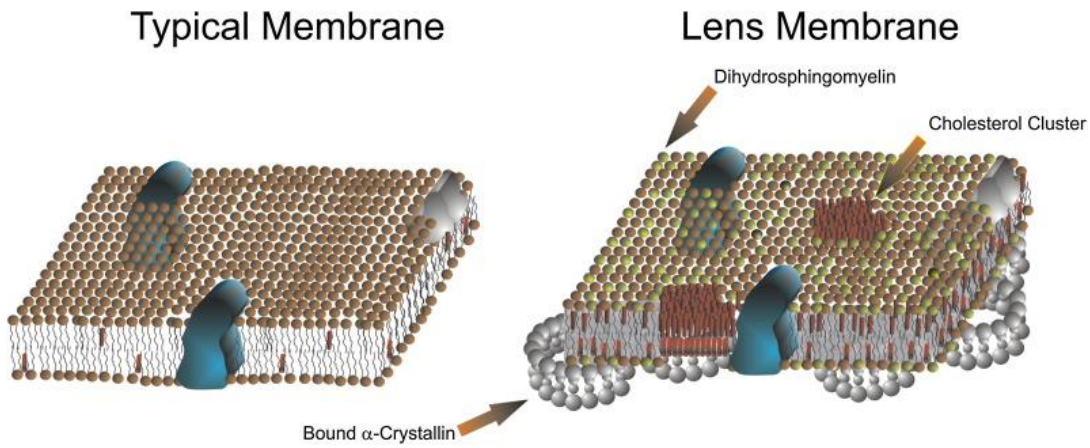

Figure 7: Comparison of Typical and Lens Membrane Structure : Comparatively high levels of Cholesterol in the eye lens lead to Cholesterol bilayer patch formation (right), and most lipids are associated with proteins such as α-Crystallin, limiting their lateral mobility. Image taken from the paper by Borchman [20].

2.2.1.1 Phospholipids

The most abundant phospholipid present in the human lens is dihydrosphingomyelin (DHSM), a variant of sphingomyelin (Figure 8) – comparable levels are only found in other primate species. [21] It is the only phosphosphingolipid found in mammals and is extremely stable, to the point where it has been observed as the only remaining lipid found in frozen mammoth tissue 40,000 years after the animal's death [22]

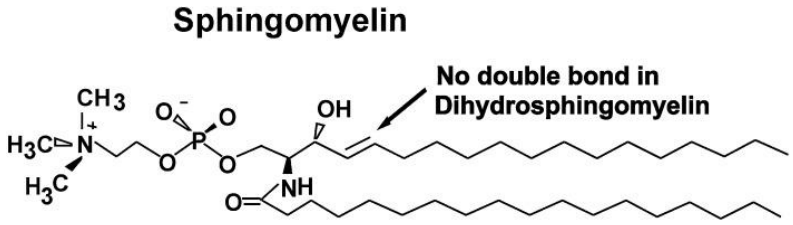

Figure 8: Structure of Sphingomyelin/ Dihydrosphingomyelin (SM/DHSM). SM consists of a phosphocholine head group, a sphingosine, and a fatty acid tail with a single double bond, which is absent in DHSM. Image taken from the paper by Borchman [20].

Phospholipid content in healthy adult lenses is relatively constant in all but the inner nuclear regions of the lens, where levels drop from 22-24 μg/ mg (dry weight) to around 7 μg/ mg [23].

2.2.1.2 Cholesterol

Cholesterol consists of four strongly hydrophobic hydrocarbon rings, with a weakly hydrophilic hydroxyl group attached to one end of the molecule that makes cholesterol amphipathic (Figure 9). It is an essential component in the regulation of membrane fluidity and heterogeneity in many types of cell membranes, and also assists in regulating protein-membrane association and functions [24]. It is relatively stable to oxidation when compared

with unsaturated lipids; an important factor in the eye lens where there is negligible turnover [20].

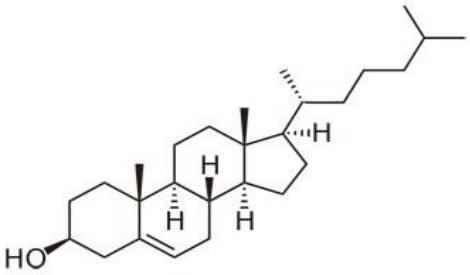

Figure 9: Cholesterol structure, taken from the site world of molecules [25]. Cholesterol molecules are amphipathic, with a hydroxyl group at one end and a set of fused steroid ring structures that give cholesterol a stiff, flat moiety.

Cholesterol molecules have a flat and stiff steroid moiety; the fused steroid rings are rigid and can be intercalated between the fatty acid chains of phospholipids in membranes. This promotes conformational order of phospholipids in the vicinity by increasing the number of trans lipid rotamers (rotational isomers) present (Figure 10), enabling tighter packing and maximum Van der Waal's (VDW) interactions between adjacent lipids [26].

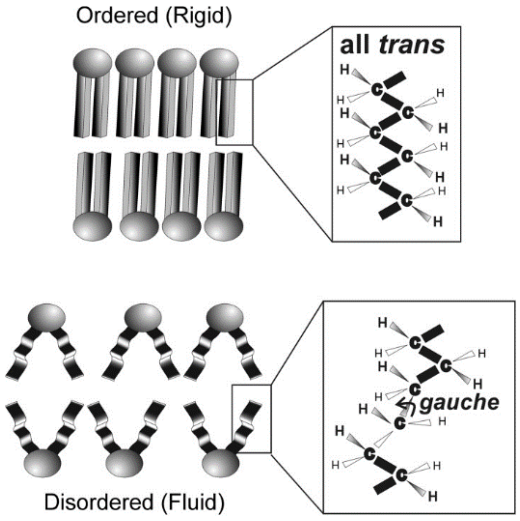

Figure 10: Conformational order in membranes. Cholesterol in disordered membranes intercalates between the fatty acid chains of phospholipids in membranes, promoting more lipids to become more ordered trans rotamers and ordering the membrane. Taken from the paper by Borchman [20].

This ordering effect is dependent on the planar α-face made by the steroid rings; if perturbed, for example by the inclusion of methyl groups in Cholesterol precursor Lanosterol, the ordering effect is diminished – meaning lanosterol cannot act as a substitute for Cholesterol

in biological membranes [27]. Increasing membrane order decreases membrane elasticity and allows less access of small water-soluble molecules through the membrane.

Experiments using pulsed field gradient NMR (Nuclear magnetic resonance) have been used to observe how varying the percentage of cholesterol affects lateral lipid diffusion in membranes (up to 40 mol%) – generally, the lateral lipid diffusion coefficient (related to fluidity) decreases linearly with increasing Cholesterol concentration in membranes in the L_D phase largely composed of phosphotidylcholines (PC), but is almost independent of Cholesterol levels in (SM) sphingolipid systems. The L_O state does not share this dependence.

The eye lens membranes have the highest cholesterol content in the human body. Levels increase from 14μg/mg in the OC to 25μg/mg in the nucleus (dry weight) – even in the cortex this is very high compared to other body tissues. For example, the outer cortex has a molar cholesterol-phospholipid ratio of 1:2 - compare with membranes of the muscle sarcoplasmic reticulum, which may have cholesterol: phospholipid ratios as low as 2:25 [28]. Within the inner nucleus(IN) cholesterol levels do drop, but the ratio of cholesterol: phospholipid continues to increase as phospholipid levels drop off more rapidly [23].

Fourier Transform Infrared (FTIR) spectroscopy has been used to show that Cholesterol functions in the eye lens to maintain a similar lipid ordering throughout; in biologically-present concentrations, Cholesterol in eye lens membranes increases the structural order of cortical membrane lipids and decreases the order of nuclear [29].

Rafts

Cholesterol is not usually distributed uniformly throughout cell membranes; it forms micro or nanodomain 'rafts'. These are defined as small (10-200 nm across), highly dynamic domains that are rich in cholesterol and sphingolipids, and which compartmentalise cellular processes [30]. The concept evolved from the observation of insoluble complex formation following membrane solubilization with mild detergent (Triton X-100) [26].

Cholesterol intercalates between the sphingolipid saturated hydrocarbon tails to condense the membrane as described previously – this forms small regions of liquid ordered (L_o) phase as rafts in the liquid disordered (L_d) bilayer [31]. Observations of two-phase regions within SM/cholesterol model bilayers show a rapid exchange between L_d and L_o bilayer regions on an NMR timescale (100 ms), showing formation within a single lipid bilayer of these highly ordered, sub-millimetre scale fluid domains. Bilayers not containing SM did not exhibit two-phase behaviour [32]. Many proteins have been suggested to be associated with lipid rafts, indicating they play an important role for membrane-associated protein functioning [33].

Cholesterol-rich rafts have been reported in human lens membranes treated with mild detergent and sucrose density centrifugation – non-sedimenting fractions with raised cholesterol: lipid ratio appeared only in samples from clear (non-cataractous) lenses despite minimal difference in phospholipid content, indicating disruption to these regions occurs in cataract [5].

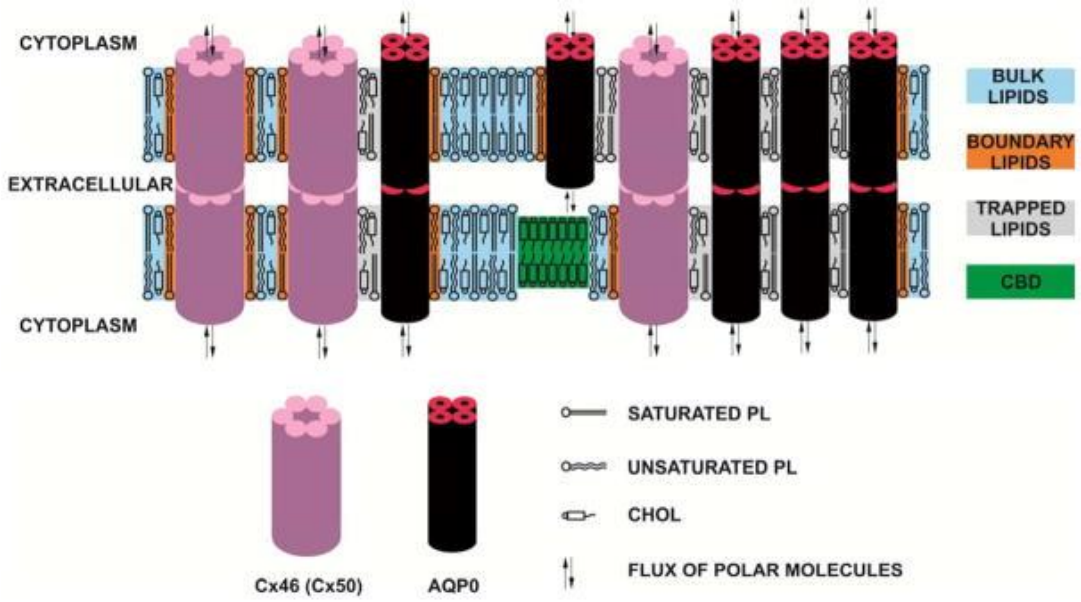

Figure 11: Lens membrane lipid domain organisation. Three distinct lipid environments have been observed in the lens; bulk lipids (blue), boundary lipids surrounding protein-rich regions (orange) and trapped lipid domains between proteins in arrays (grey). The presence of cholesterol boundary domains (CBD, green) is possible due to high cholesterol content in lens membranes. Taken from the paper by Subczynski [34].

Observation of intact membranes shows three distinct lipid environments; the bulk, boundary domain around the edge of protein-rich regions (which cholesterol is absent from) and trapped lipid domains between proteins in the array (Figure 11) [34].

Bilayer Domains

The saturation of cholesterol in the eye lens is high enough to allow for the formation of cholesterol bilayer domains (CBDs). CBDs have yet to be observed in intact lipid membranes, but Electron Paramagnetic Spin-Labelling (EPSL) has been used to observe cholesterol bilayer domains in extracted human lens lipids and membrane models overloaded with cholesterol. Profiles were taken of phospholipid chain order, fluidity, oxygen transport parameter, and hydrophobicity. These domains are distinct from phospholipid-cholesterol and cholesterol-enriched raft domains - they act as a buffer for cholesterol concentration in the surrounding phospholipid: cholesterol domains, keeping a constant saturation level and maintaining the physical properties of the membrane when phospholipid content undergoes changes [35].

The amount of CBD in nuclear membranes is higher than in cortical extracts, consistent with higher cholesterol: phospholipid ratio. These domains also show a very low permeability to oxygen, which would act as an oxygen transport barrier across fibre cell membranes, possibly to minimise oxidative damage [36].

2.2.2 Proteins of the Eye Lens

The LFCs contain a high concentration of proteins, approximately 300mg/ml - this initially seems surprising in a transparent tissue. In fact, this high concentration is necessary for tissue transparency, as well as for determining the refractile properties of the lens.

The protein composition of bovine lens cortical membranes was examined by electrophoretic analysis of urea-insoluble membrane regions in 1975 – seven major protein components were identified [37]. Later, more comprehensive proteomic analysis of lens lipid raft domains identified the presence of around 500 proteins, 71 of which were observed to be strongly affected by cholesterol removal. These included water channel proteins, raft markers (flotillins) and some connexins [38]. Membrane proteins in the eye lens are largely located close together in junctional domains associated with cholesterol-enriched lipid fractions (Figure 11). These protein assemblies have been observed using thin-section transmission electron microscopy (TEM) of gold-labelled samples [39, 40].

Proteins in the eye lens must resist damage by exposure to UV light and reactive oxygen species for decades, or risk clouding and cataract formation – ionising radiation in excess can cause modifications to protein structure, and has been shown to contribute to cataract formation [41].

2.2.2.1 Crystallins

90% of the water-soluble protein content of the lens is made up of crystallins. These are evolutionarily linked to stress proteins and come in two main families; the α-crystallins which act as molecular chaperones and help prevent aberrant protein interactions [42], and βγ-crystallins, which are sub-classified as β- and γ-crystallins. In the human lens, α- and β -crystallins are found as oligomers and γ-crystallins as monomers [43]. The crystallins are comprised of highly related sequences - α-crystallins comprised of two, β-crystallins six and γ-crystallins [44].

Crystallins are vital to lens transparency; originally it was suggested they minimised light scatter by being in a 'paracrystalline state' [45], but later small angle X-ray scattering was used to demonstrate a lack of spatial order at high protein concentration – this showed that

short-range, liquid-like order without large-scale fluctuations was sufficient to explain lens transparency [46].

Crystallins are also likely to be involved in maintaining the thermal stability of the lens; the lenses of arctic fish do not form cold cataracts in water temperatures below freezing, and analysis of their lenses showed raised levels of γ crystallin (>40% of crystallin content) compared to bovine lenses [47].

2.2.2.2 (BFSP1) Beaded Filament Structural Protein 1

The BFSP1 gene encodes the protein filensin in humans; it a membrane-associated cytoskeletal element. Mutations in this gene result in an autosomal recessive disease, causing juvenile-onset cataract that is restricted to the cortex of the lens. The gene and its protein products are not simple; it has 7 exons, 2 promoters, 3 protein start sites and several predicted caspase cleavage sites [48]. Several different isoforms have been identified from transcript variants.

The isoforms are expressed in a tissue-specific manner; in the eye lens membrane the protein is resistant to extraction, indicating it acts as an integral membrane protein. This is consistent with amphipathic helix structures that form transmembrane domains, and so the interaction of the correctly and incorrectly cleaved variants of this protein with lens membranes is an area of interest.

Filensin has been observed to interact with the C-terminus of AQP0; chemical cross-linking study showed this occurs increasingly in fibre cells with age, in the same regions of the lens where truncation of filensin is seen. This data suggests the interaction occurs near to the major truncation site located in the C-terminal tail of filensin, indicating it may play different roles in developing and ageing lenses [49].

2.2.2.3 Aquaporin 0 (AQP0)

Previously known as Major Intrinsic Protein (MIP), AQP0 constitutes around 50% of total LFC membrane proteins; it comes from a family of membrane pores that allow the passage of water or small uncharged solutes only [50]. In the lens it functions as a water channel protein and plays a role in cellular adhesion (Figure 12 a-c). Specific control of function is regulated through pH, Ca^{2+}/ calmodulin and C-terminal cleavage [51].

Post translational modifications are implicated in AQP0 function in the lens; in particular the phosphorylation of Serine 235 – this allows a stable complex to be formed with A-kinase anchoring protein 2 (AKAP2) and is involved in preserving lens transparency [52]. Backbone cleavage has also been observed at residues 246 and 259 – this may result from nonenzymatic truncation at Asp residues. Matrix-Assisted Laser Desorption/Ionization-Time Of Flight

(MALDI-TOF) mass spectrometry and SDS-PAGE analysis of mouse lenses showed cleaved AQP0 does not appear in the outer cortex LFCs, but increases progressively deeper into the lens until only cleaved forms appear in the nucleus [53].

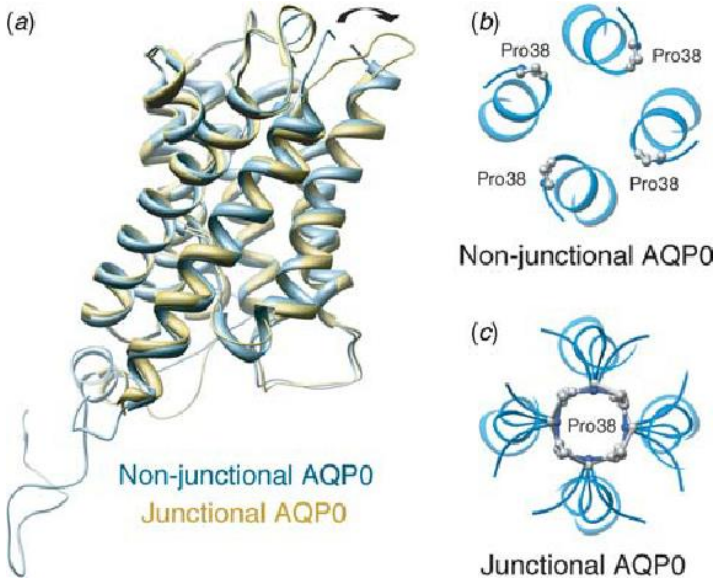

Figure 12: AQP0 non-junctional and junctional structures. a) Comparison of AQP0 forms. b) Non-junctional AQP0, which acts as a water channel in lens membranes. c) Junctional AQP0 structure, which plays a role in cellular adhesion. It features centrally facing Pro38 residues. Figure taken from the paper by Gonen [54].

AQP0 deficiency has been observed to cause uncontrolled elongation, fragmentation and deformation of protrusions in maturing LFCs of mouse models (although overall cell shape remained the same). This later led to fibre cells separating and breaking down, resulting in cataract formation in the lens core. In humans, several mutations in AQP0 have been observed to cause congenital cataract formation [55].

Studies suggest AQP0 in the roles of controlling membrane transport and interactions is important in LFC development and maintenance of the interlocking structures at the cell boundaries that are important in maintaining lens transparency and integrity [56]. Partial AQP0 knockouts cause spherical aberration, increased light scatter and cataract, which could not be rescued by restoring water permeability of cell membranes, and electron micrographs showed increased extracellular space between LFCs, showing the structural importance of AQP0 during lens development [53]. Loss of one or both AQP0 alleles also causes a significant reduction in resistance to compressive forces when compared to wild type lenses [57].

Water channel

AQP0 has a relatively low permeability for water when in neutral pH conditions – 40 times lower than AQP1, for example [58]. However, under mildly acidic conditions such as those

in the core of the eye lens (pH 6-6.5 at 37 °C), this permeability can increase two to four-fold as the formation of AQP0 orthogonal arrays is induced [59]. This effect is believed to be modulated by the binding of H^+ to a histidine residue in the first extracellular loop of AQP0, a residue that is not present in the pH-insensitive AQP1 [51]. Shifting or replacing these loops has been demonstrated to change how pH affects water permeability of the channels using bovine AQP0 [60].

Junctional

Modification to the C-terminal of AQP0 induces the formation of gap junctions through interaction of AQP0 tetramers in neighbouring cells – these form tight junctions with closed water pores (Figure 13), meaning AQP0 is playing a structural role when in this configuration [61].

Junctional AQP0 interacts with structural membrane proteins; it co-localises with the gap-junction forming connexin proteins, shown in developing chick lenses by immunoprecipitation and immunoblotting experiments. This co-localisation diminishes in mature lenses apart from in the actively dividing bow regions of the lens, indicating an important interaction occurs between AQP0 and connexins during development [62].

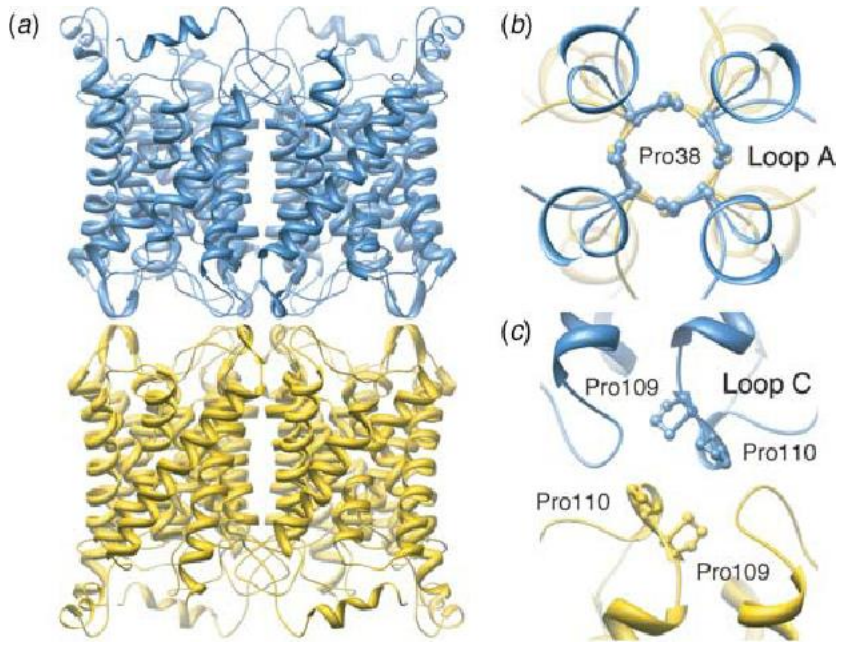

Figure 13: Junctional AQP0 structure and function. C-terminus modification induces interaction of AQP0 tetramers in neighbouring cells, forming tight junctions between them which do not act as water pores. Figure taken from the paper by Gonen [61].

AQP0 has also been observed to colocalize with the cytoskeletal proteins filensin (BFSP1) and CP49, using immunoprecipitation and the AQP0 C-terminus in a pull-down experiment.

Specific colocalization at cell membranes was confirmed using immunofluorescence confocal microscopy and immunoelectron microscopy [63]. Co-immunoprecipitation and pull-down experiments also linked the AQP0 C-terminus with ezrin, radixin and moesin (in particular ezrin), proteins involved in linking actin filaments to cell membranes, fibre cell elongation, organisation and morphology [64]. Together, these experiments indicate AQP0 plays an important role in LFC structuring via cell membrane located interactions.

Using yeast two-hybrid screening and co-immunoprecipitation it has been shown that AQP0 (specifically the C-terminus) interacts with γE-crystallin, which is specific to LFCs [65].

2.2.2.4 Connexins

Connexins (Cx) are a set of structurally-related transmembrane proteins, which co-assemble into oligomers of six connexins to form a connexon or hemi-channel (Figure 14). This connexon can then dock with another connexon from an adjacent cell to form a gap junction channel [66]. Gap junctions bridge the membranes of adjacent cells, to allow direct cell to cell communications through the transfer of ions and small solutes (≤1kDa in size), and hemichannels control metabolite flux between the interior of cells and the extracellular space surrounding them [67].

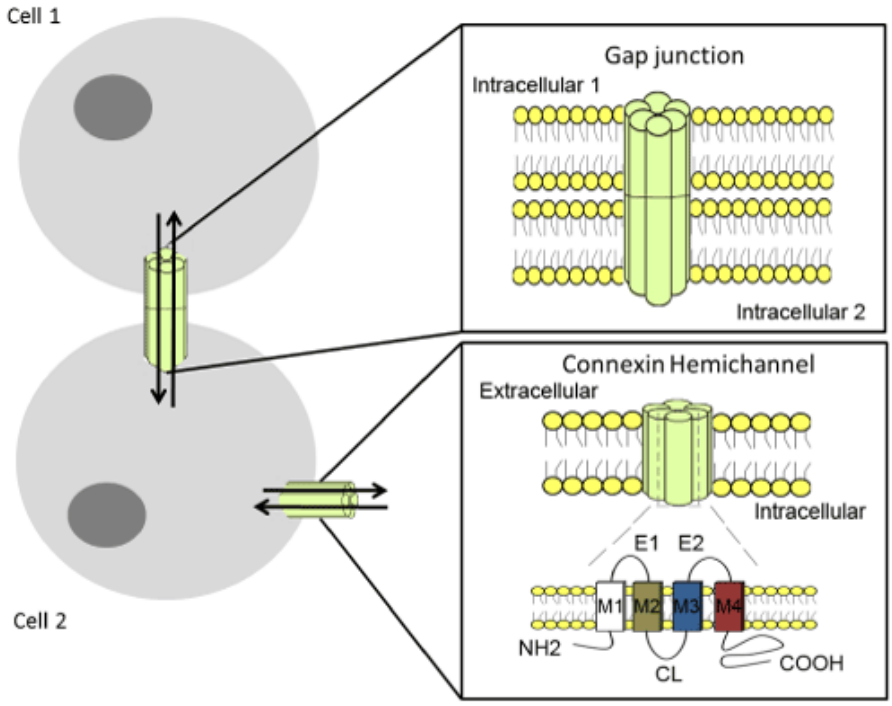

Figure 14: Connexin forms gap junctions and hemichannels. Groups of six connexins form co-assemble to form connexons/hemichannels, which can pair with connexons in the membrane of neighbouring cells to form gap junctions. Image taken from the paper by Retamal [68].

In the human eye lens, connexins Cx43, Cx46, and Cx50 are present; collectively they constitute over 10% of total LFC membrane protein content [69]. Together with AQP0 they form a network of gap and tight junctions (Figure 15) that provides the tight packing of LFCs necessary for transparency, as well as transport of water and small molecules through the body of the lens. The formation of boundary and trapped lipids in LFC membranes (Figure 11) is likely induced by the arrangement of thin AQP0 junctions and Connexin gap junctions.

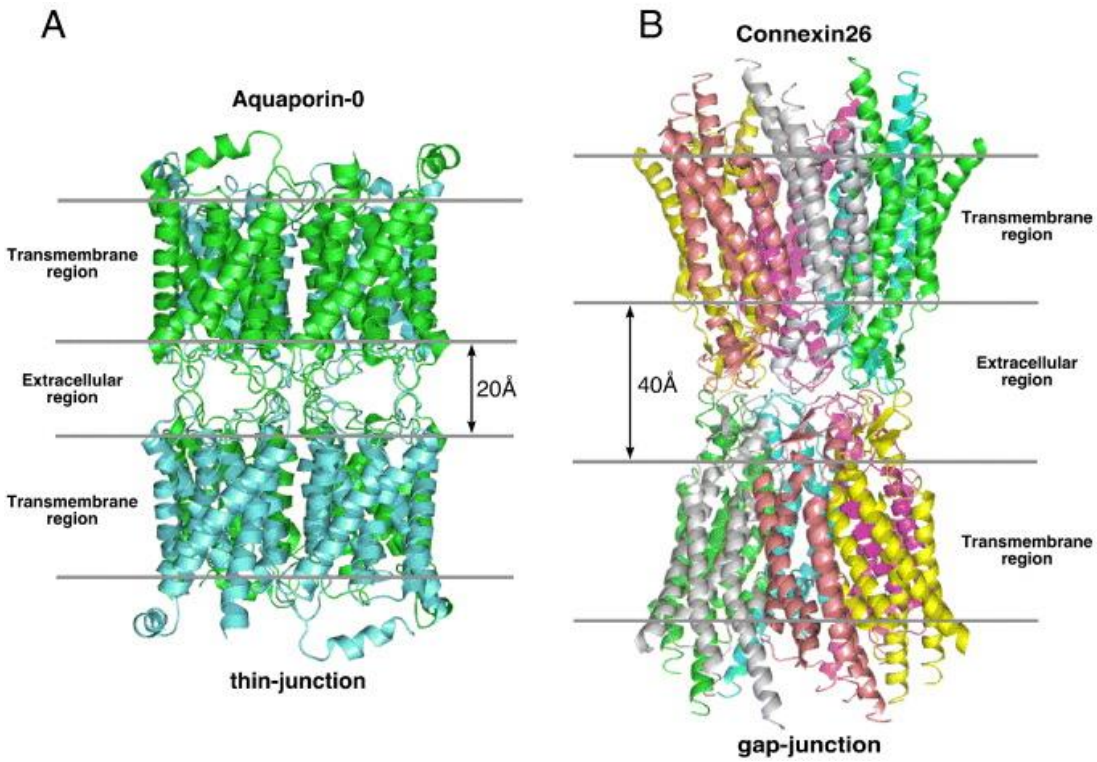

Figure 15: Eye lens membrane proteins AQP0 and connexin form head-to-head junctions. AQP0 tight junctions and Connexin gap junctions form a network that provides the tight packing of LFCs necessary for transparency. Mutant versions have been linked to congenital cataract formation. Image taken from the paper by Buzhynskyy [70].

Mutant versions of these connexins have been linked to congenital cataracts, with aberrant voltage gating of hemichannels or modulation by divalent cations. They may also play a role in age and disease-related cataracts if protein function is compromised with time or damage.

High resolution AFM has been used to observe the organisation of these proteins into microdomains, using native lens extracts from the IN region of the lens – AQP0 forms square arrays that are surrounded by densely-packed gap junctions (Figure 16). These structural groups keep tight spacing between LFCs, as well as providing adhesion and communication. The topography shows the conformation of the extracellular loops of AQP0 in these arrays matches the structure of junctional AQP0 formations, with closed water pores [71].

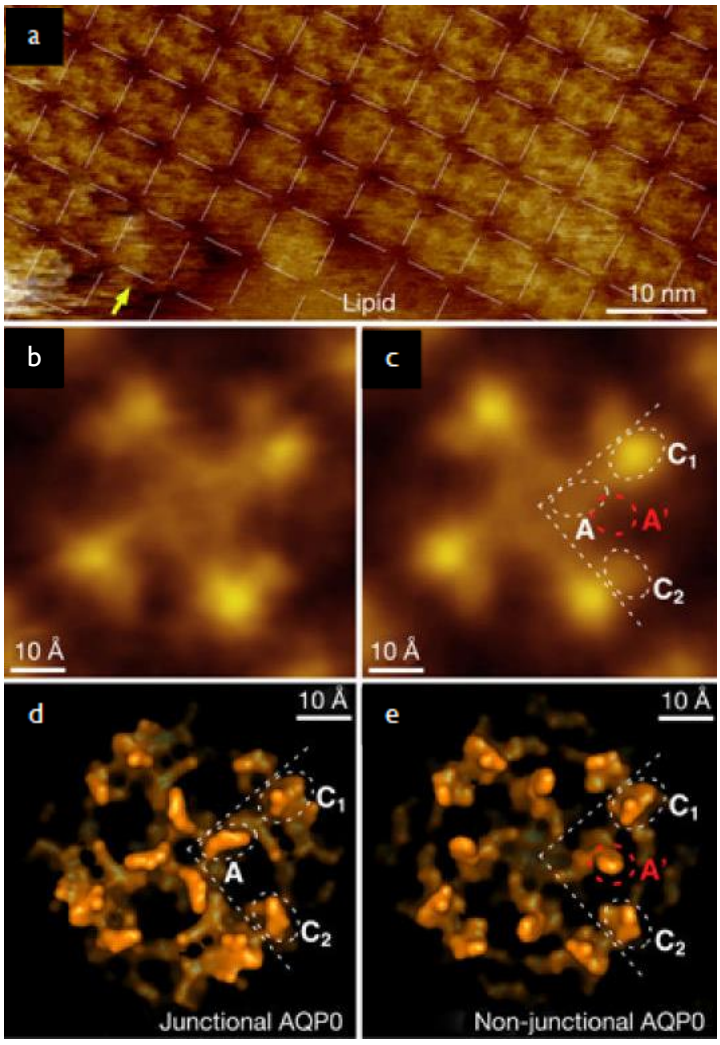

Figure 16: High resolution AFM imaging of AQP0 arrays. a) The square array arrangement of AQP0 tetramers is highly organised in structure, and is vital to keeping the tight spacing between adjacent lens fibre cells required for transparency. Also visible at this resolution is the the conformation of the extracellular loops of AQP0, which match the structure of junctional AQP0 (b-e) Image adapted from the paper by Buzhynskyy [71].

2.2.3 Membrane Interactions

The interactions between protein and membrane are vital to a variety of processes such as membrane trafficking, cell-cell communication, control of membrane fluidity and changing of membrane shape to form protrusions (including filopodia and lamellipodia). Some mechanisms are not fully understood yet, but new insights into the biophysical properties of membranes and their interactions – the 2D and 3D structure, physical properties, dynamics and activity of systems can be explored through an ever-expanding variety of methods.

2.3 The Ageing Lens

2.3.1 Lipids

As the lens ages oxidative damage accumulates over time - long term exposure to radiation from the sun, among other sources, can cause oxidation of the membrane lipids. The lens lipids have negligible turnover rates across decades of lifespan and so are not typically replaced if damaged – this negligible turnover was demonstrated by Hughes [72], who showed Carbon-14 levels in the lipid content of lens nuclei give accurate predictions of an individual's age (matching atmospheric levels at the time).

Magnetic resonance spectroscopy has been used to observe changes to the lens lipidome as it ages; in humans, levels of sphingolipids such as dihydrosphingomyelin increase relative to glycerolipids including phosphatidylcholine (Table 1). Damage to the lens and cataract exacerbates this effect, with cataracts having the greatest change in lipid levels of any known disease [73] .

Table 1: Distinct changes occur in the lens lipidome with increasing age, with levels of sphingolipids (DHSM, SM) increasing relative to glycerolipids (PC, PE, LPE, PS). Table copied from the 2012 paper by Hughes [74].

Lipid Class	*Percentage of Total Lipid (%)*		
	Foetal Lens	Young Lens (10-20 years)	Old Lens (70-80 years)
DHSM (dihydrosphingomyelin)	9.7	36±2.5	35±0.4
SM (sphingomyelin)	3.0	8.8±0.6	9.8±1.7
PC (phospatidylcholine)	50	1.2±0.1	0.6±0.2
PE (phosphatidylethanolamine)	27	19±3.1	3.1±1.5
LPE (lysophosphatidylethanolamine)	0.5	29±3.0	19±1.3
PS (phosphatidylserine)	10	5.7±1.4	1.3±0.5
DHCer (dihydroceramide)	0.3	0.2±0.0	22±4.0
Cer (ceramide)	0.3	0.1±0.0	8.0±1.4

In a tissue with no lipid turnover, more unsaturated lipids with fewer double bonds are less resistant to oxidation – the rate constant for the propagation step of lipid oxidation drops when the number of double bonds is reduced [75]. Sphingolipids are three to four times more saturated than glycerolipids such as phosphatidylcholines, and consequently outlast them as they are much less susceptible to oxidation [76].

This change in relative lipid content means there is an overall increase in lipid hydrocarbon chain order, and therefore stiffness, of the lens membranes. This effect is also more apparent in cataractous lenses. This increasing stiffness of the ageing membranes may contribute to increasing light scattering, slowing of LFC elongation and deleterious alteration of protein-lipid interactions.[73]

A key change to the makeup of the lens is observed during middle age; Matrix Assisted Laser Desorption/Ionization (MALDI) mass spectrometry has been used to observe that DHSM levels between the cortex and nuclear regions increase until around age 40, at which point a plateau appears – this 'barrier region' may act as an internal block to the diffusion of small molecules in the lens, and is hypothesized to be an important event in the development of age-related nuclear cataracts [77].

Also notably, electrospray ionization tandem mass spectrometry showed the appearance of dihydro/ceramide (DH/Cer) in lenses in significant levels only after the age of around 30 and increase 100-fold over the course of life – ceramides have been shown to cause the death of lens epithelial cells in small concentrations in culture, so their presence in the lens could be related to alteration of normal metabolic processes in the lens [78].

The sphingomyelin content of different species varies tremendously, and high percentages of this long-lived lipid likely convey some resistance to cataract formation with ageing; Organisms with long lifespans such as humans and bowhead whales [79], as well as organisms with slightly shorter lifespans that are known for very rarely developing cataract such as camels, tend to have a high proportion of sphingolipids present in their eye lens membranes [21]. In the bowhead whale, for example, animals can survive for upwards of 200 years and never develop cataracts.

No lipids are immune to oxidative damage entirely, however; as the lens ages, lipid oxidation products appear in increasing concentration in the lens. Particularly notable are the oxidation products of Cholesterol, known collectively as oxysterols (Figure 17). Oxysterols differ from cholesterol by having additional functional polar groups, usually hydroxyl, keto, hydroperoxyl, epoxy or carboxyl moieties [24] – these groups significantly change the biophysical properties of membranes and have been shown to accumulate in human lenses with age [74].

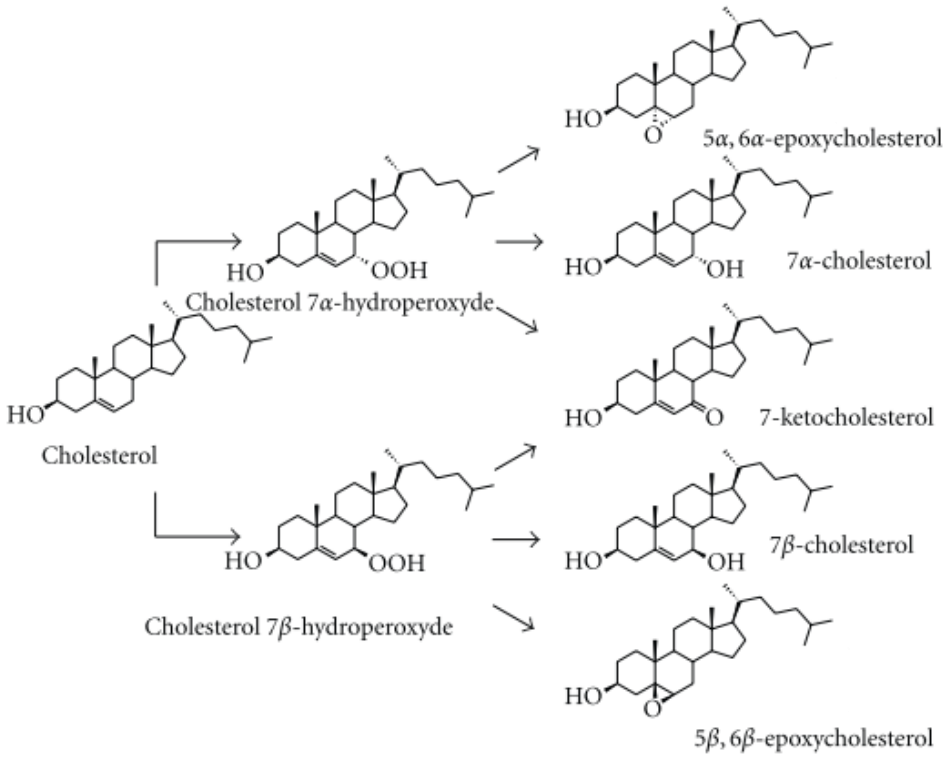

Figure 17: Cholesterol oxidation products. Cholesterol can be altered through natural and artificial means to form a variety of oxidation products including 7-ketocholesterol, which appears at raised levels in cataractous lenses. Figure adapted from the paper by Vejux [80].

The most abundant oxysterol in the human eye lens is 7-ketocholesterol; this differs from cholesterol by the addition of a ketone functional group at the 7th position, on one of the hydrocarbon rings (Figure 18).

As mentioned in previously, Cholesterol relies on the flat, stiff steroid moiety conveyed by the planar structure of its α-face to convey its lipid ordering properties, promoting tighter lipid packing, decreasing membrane elasticity and making the membrane an effective barrier to small water-soluble molecules [81]. 7-ketocholesterol having an additional double bonded oxygen present within this structure is likely to affect the function of Cholesterol by altering the interaction with membrane components and therefore the overall membrane properties, as well as how effectively protein-membrane interactions can occur.

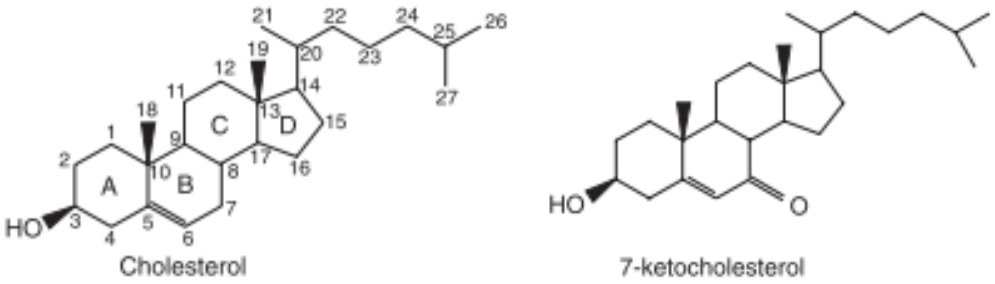

Figure 18: Cholesterol and 7-ketocholesterol structural comparison - note the double-bonded oxygen at the 7 ring position, which would normally be the flat, planar section of the molecule that allows it to intercalate effectively between membrane lipids. Adapted from the paper by Lyons [82].

Oxysterols are implicated in diseases - age-related or caused by excessive oxidative stress, such as smoking, diabetes and excessive exposure to sunlight [83]. Chronic exposure to UV light and ozone can also lead to the formation of certain oxysterols, [84] and raised levels are found in cataractous lens membranes. Acting as markers for oxidative stress, the lens lipid compositional changes can also be related to how healthy an individual is as they age, and how long they are likely to live for [20].

2.3.2 Proteins

Proteins in the lens must also survive for decades with no turnover, as the differentiated LFCs lack the required machinery to produce more. Over time, post-translational modifications (PTMs) accumulate in the ageing lens proteins, with the most abundant PTM being racemization. Also known to occur are the cleavage of peptide bonds, formation of cross-links, deamidation and other forms of isomerism. These PTMs can occur spontaneously with age; with Serine, Aspartic acid, Asparagine and Serine phosphate amino acids particularly susceptible to decomposition. They can also be induced by metabolites – some biomolecules can covalently attach to proteins, modifying them [85].

As the frequency of PTMs increases, lens proteins become progressively less soluble – this can disrupt protein-protein or protein-membrane interactions and cause increased light scattering [85].

Crystallins are extremely stable proteins – useful in the lens as they must endure for much longer than proteins in fast-cycling tissues; nevertheless, they do eventually accumulate post translational modifications such as deamination and truncation [86]. These PTMs interfere with the strength of short-range protein-protein interactions and decrease transparency [87]; changes in interaction strength between alpha, beta and gamma crystallins have been

observed in mutant proteins associated with cataractogenesis using methods including surface plasmon resonance [88].

As with the cellular lipidome, important changes to the proteins of the eye lens occur during middle age. Starting at around age 40, soluble α-crystallin levels decrease and additional structures appear containing crystallins and membrane lipids – denatured α-crystallin has been shown to bind to LFC membranes. The observations made are consistent with binding of crystallin aggregates to LFC membranes on a large scale during middle age in humans [89]. The majority of beta (with the exception of chaperone protein α-B-crystallin) and all gamma crystallins become increasingly membrane-bound with age; these could contribute to the impairment of cell-cell communication if they interrupt junctions [90].

2.3.3 Lens Defects

As the lens ages and accumulates modifications to constituent lipids and proteins, the risk of developing diseases that can negatively impact vision increases alongside. Most people will develop presbyopia, an inability of the eye lens to accommodate enough to focus on close objects. around middle age and if an individual lives long enough they will eventually develop cataracts, a clouding of the eye lenses that causes distortion of vision and eventually vision loss.

2.3.3.1 Cataract

Cataracts can develop for a variety of different reasons, including radiation exposure, physical trauma, congenital defects and as part of the normal ageing process - Eventually everyone would develop cataracts if they lived long enough, but a variety of factors can increase the likelihood of cataract development earlier in life. These can be genetic, associated with lifestyle factors that increase the rate of oxidative damage to the lens (such as excessive UV exposure or smoking), previous eye injury, inflammation or surgery, hypertension or steroid medication use.[83]

Morphological defects of the LFCs have been observed in human aged normal and age-related cataractous lenses, but cataractous lenses have been observed to contain more irregularly shaped fibre cells, with membranes that are convoluted and irregularly structured.

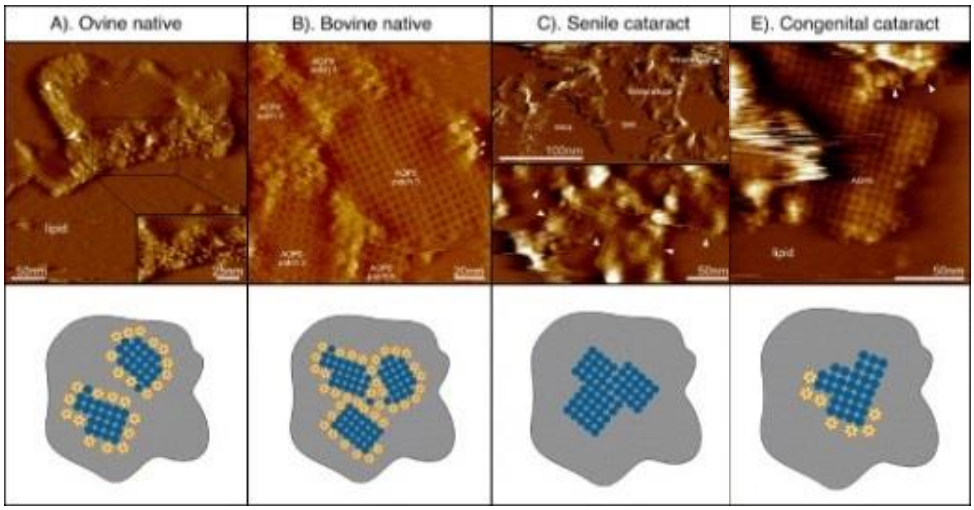

Figure 19: Arrangement of AQP0 and connexins in healthy and cataractous lens membranes, adapted from the paper by Buzhynskyy [70]**. In all lenses, AQP0 (blue dots) clusters in ordered arrays, but in the senile cataract the connexons (yellow circles) that would normally surround the AQP0 clusters is absent.**

Human cataractous lens membranes have been mapped at sub-nanometre resolution using AFM to view how the arrangement of junctional microdomains differs from healthy lenses; instead of the characteristic AQP0 square arrays surrounded by gap junctions individual AQP0 tetramers were present with no associated connexon (Figure 19). These defects of structure indicate the membranes are likely to be less capable of metabolite transport and waste product removal via the internal circulation of the lens, and disruption to the adhesion of adjacent cell membranes due to the loss of order in junctional protein structures (Figure 20). In the case of some congenital cataracts, however, there appears to be no visual difference in the arrangement of channel proteins to healthy lenses (Figure 19), indicating a different feature within the lens is causing the decrease in transparency [70].

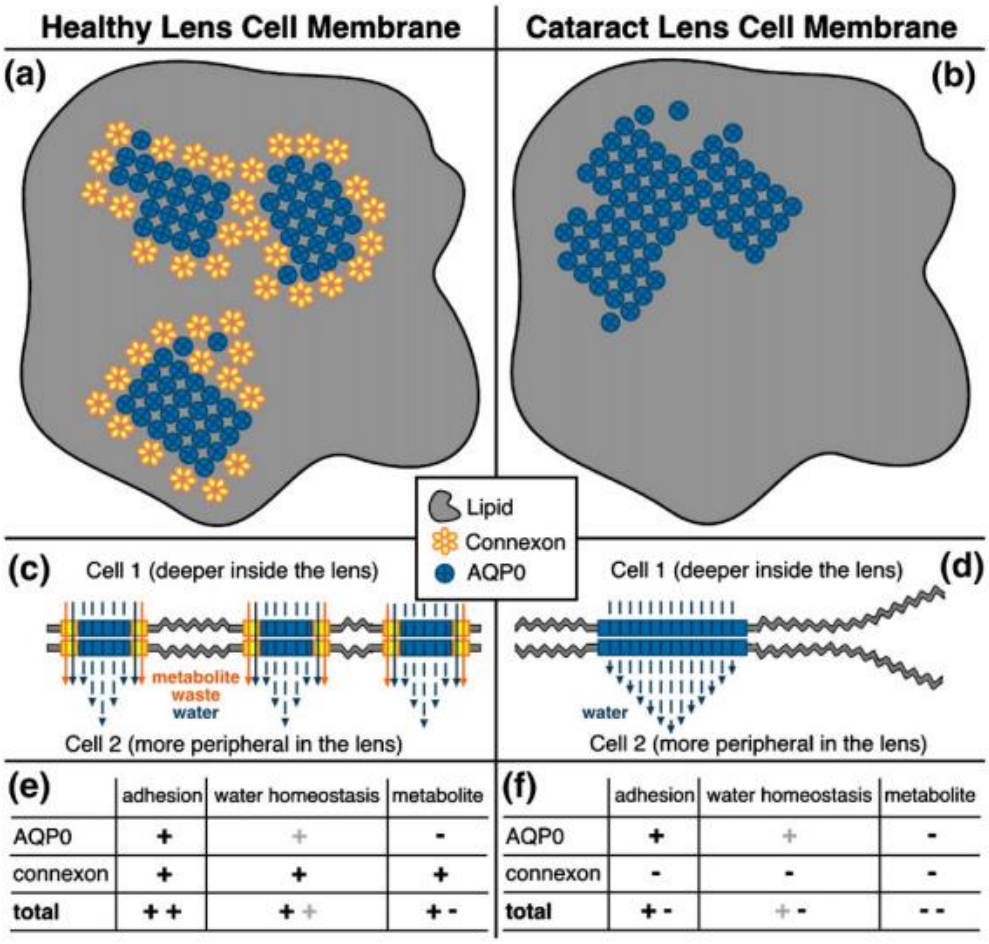

(e)

	adhesion	water homeostasis	metabolite
AQP0	+	+	-
connexon	+	+	+
total	+ +	+ +	+ -

(f)

	adhesion	water homeostasis	metabolite
AQP0	+	+	-
connexon	-	-	-
total	+ -	+ -	- -

Figure 20: Models of the supramolecular assembly of junctional microdomains in core lens membranes. In healthy lens membranes AQP0 is clustered in arrays that are surrounded by connexons, allowing effective cell-cell adhesion and homeostasis of water and metabolites. In cataractous membranes the connexons are lost and transport of water across the membrane is less well regulated. Figure taken from a paper by Buzhynskyy [70].

Oxysterols appear in cataractous lenses in raised levels – the most common in humans being 7-ketocholesterol which is present at levels of 4.2 ± 3.2 mmol mol^{-1}, whereas in young, healthy lenses the amount is negligible [7]. As cholesterol is an important component in the eye lens membrane domains, it is likely that disruption of its function in regulating membrane fluidity would disrupt the arrangement of protein structures integral to the membrane – the presence of oxysterols, which have additional groups interrupting the cholesterol structure and therefore function, is likely to be implicated in the damage to protein arrangement seen in cataractous membranes.

Multi lamellar bodies (MLBs), which consist of crystalline proteins surrounded by a lipid shell about 1-4 μm in diameter, have also been observed in morphological studies of cataracts. The lipid in these structures comes from sections of membrane that do not contain integral

membrane proteins. From imaging of lenses using optical and electron microscopy to view the density of MLBs in healthy and cataractous lens tissue it has been estimated that in a cube of side length 160 μm, only 14 MLBs are required for total loss of transparency - In a healthy lens section of the same volume only 2 MLBs would be found [91].

Metabolic diseases such as diabetes have been associated with the formation of cataract. The inability to correctly regulate metabolite levels can lead to additional oxidative damage in lens, damaging the membranes; in particular at cortical-nuclear interface. Loss of cytoplasm and condensation of the LFCs have been observed in diabetic lens nuclei, with morphological defects including MLBs, irregular spacing between adjacent fibre cells and unusual density variations [92].

Currently cataracts can only be treated via surgical removal and replacement of the entire lens – Attempts have been made to develop non-surgical methods for treating cataract, such as providing lanosterol, a precursor to cholesterol, in the form of eye drops this was shown not to reverse opacification in human lenses with age-related nuclear cataract [93].

Pharmacological Treatment of cataract could be possible in early stage cataracts if a suitable mechanism or molecule is found to regulate levels of oxysterols within the lens.

2.3.3.2 Presbyopia

The decline in accommodation ability in the ageing lens is universal; over time the lens becomes stiffer and less able to deform, so light from nearby objects can no longer be focused onto the retina (Figure 21) – this is presbyopia.

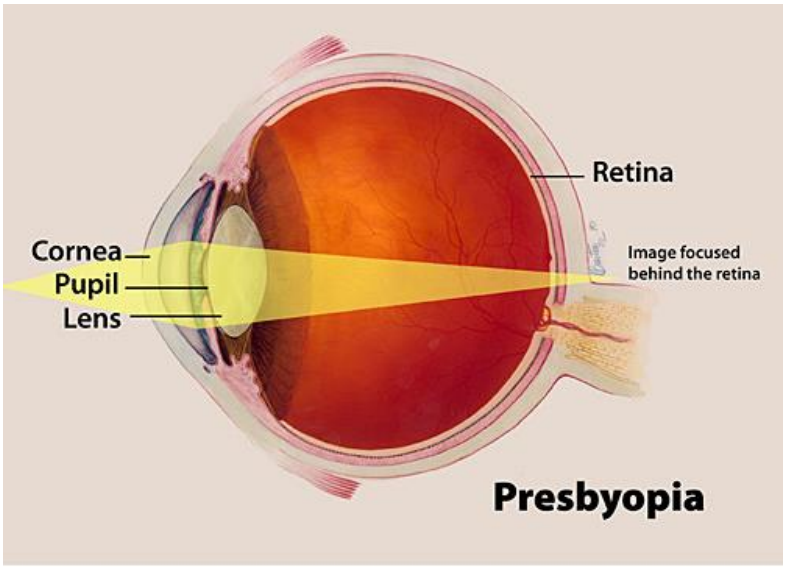

Figure 21: Presbyopiadevelops as the lens becomes stiffer and less able to deform with time, causing the light from close-up objects to be incorrectly focused behind the retina. Image taken from the National Eye Institute [9]**.**

Rotational shear experiments have observed that the stiffness of the cortex of young lenses is stiffer than the nucleus and that both cortex and nucleus become stiffer over time, but the nucleus becomes stiffer more rapidly – this means that from middle age (around the age of 45) onwards, the nucleus is stiffer than the cortex [94]. This coincides with significant changes to the lens lipidome and is around the time of presbyopia onset.

Protein aggregation is likely to be an important factor in the development of presbyopia; the protein chaperone alpha crystallin is progressively lost from the body of the cytoplasm of the LFCs as it is incorporated into high molecular weight aggregates of insoluble protein. This has been mimicked by heating pig lenses to 50 degrees Celsius to speed protein degradation, and in both this case and *in vivo* a large increase in tissue stiffness occurs [95].

It is also hypothesised that a decrease in AQP0 permeability with increasing age could be a cause of presbyopia; as the lens deforms, fluid must move though the cells and if there is a decrease in permeability to water it will increase resistance to deformation of the lens for accommodation [96].

2.4 Studying membranes and their interactions

Fluorescence Recovery After Photobleaching (FRAP)

Fluorescence Recovery After Photobleaching (FRAP) can be used to observe kinetics of diffusion in living cells and the dynamics of lipid membranes, primarily in liquid phases, as well as track lateral movement of integral membrane proteins. Lipids or proteins of interest are labelled with a fluorescent probe and the movement of these tagged components can be observed by photobleaching a small area and then imaging the fluorescence recovery over time the diffusion (or active movement in cells) can be tracked and information about the dynamics gathered.

Initially analysis of fluorescence recovery following photobleaching samples was only viable for specific bleaching geometries; first a circular Gaussian laser beam profile, and later a rectangular bleaching geometry, achieved by the development of an empirical equation to calculate diffusion coefficients. A simulation approach has now been developed by Blumenthal [97] that allows for analysis of arbitrary bleaching geometries, fitting the image data with the simulated diffusion (2D random walk) of the fluorescent probes frame-by-frame in time to extract the diffusion coefficient.

The effect of increasing cholesterol levels on the fluidity of model membranes has been investigated using FRAP (Table 2) [98] [[99]

Table 2: Lateral diffusion coefficients vary for bilayers with different lipid compositions. Adapted from the paper by Ladha [99].

Bilayer Composition	*Lateral diffusion coefficient D X 10^8 (cm^2/ s)*
POPC:DOPE (7:3)	13.3 ± 0.8
POPC:DOPE:Cholesterol (7:3:5)	6.2 ± 0.6
POPC:DOPE:Cholesterol (7:3:10)	6.2 ± 0.6
DOPC	13.4 ± 0.7
DOPC:Cholesterol (1:1)	8.9 ± 1.1

X-Ray Crystallography has long been a useful tool in determining the likely structures and functional domains of proteins. The structure of the lens membrane has also been examined through X-ray diffraction analysis, showing high levels of cholesterol, typical of this tissue, forming sterol-rich domains that remained structurally constant across a wider temperature range than the sterol-poor phase [100]. This method also requires the protein to be crystallised, makes it unsuitable in observing dynamic interactions.

DNA/protein sequencing can be useful for identifying structural features that can predict protein functions – tools such as the Basic Local Alignment Search Tool (BLAST) quickly identify sequence similarities of nucleotide or protein order in known proteins and structural domains, and can be used to identify similar features in new sequences that can predict behaviour of structures.

2.4.1 Single molecule analysis methods

Historically, attempts to study membrane-protein interactions rely on there being many protein molecules, and these run into issues when attempting to observe interactions under applied mechanical force - specific, synchronised force to membranes or proteins is difficult to achieve when many proteins are involved. Single molecule analysis methods can move beyond these issues to allow observation of single protein-membrane interactions with greater precision.

2.4.1.1 Single molecule force spectroscopy using optical tweezers

Single-molecule force spectroscopy using optical tweezers has been used to quantify the binding energy of membranes and single proteins. Tightly focused laser beams are used to trap silica or polystyrene beads in a harmonic potential; the beads can then apply forces (0.02-250 pN) to a single attached protein. Applications have included quantifying membrane

binding strength and kinetics with force application to C2 domains in Synaptotagmin-1 (Syt1) and Extended Synaptotagmin-2 (E-Syt2) with varying concentrations of calcium ions, salt and other potential inhibitors present [101]. This method is suitable for 3-D manipulation and provides excellent spatial resolution (0.1–2 nm), but is not suitable for higher force interactions, and can cause undesirable sample heating and photodamage. There is also no selectivity or exclusivity control in trapping objects – any dielectric particles nearby the laser will be trapped, and there may be many trapped at once, unintentionally [102].

2.4.1.2 Magnetic Tweezers

Magnetic Tweezers are simpler to assemble than other systems; a basic MT consists of a pair of permanent magnets positioned above the sample, with an attached CCD (charge coupled device) camera. Magnetic tweezers can be used to rotate and move magnetic particles highly selectively, without disturbing the sample. They allow for force clamping over large distances, which has made them useful in observations of DNA twisting, torque and extension [103], but more versatile methods are preferred for observing membrane-protein interactions

2.4.1.3 Atomic Force Microscopy

Atomic Force Microscopy (AFM) is a type of scanning probe microscopy, advantageous for imaging membrane samples in close to physiological (aqueous) environments, at biologically-relevant temperatures, with sub-nanometre resolution and without requiring invasive preparations required by other high-resolution imaging methods, such as vacuum conditions, freezing or chemical fixing [104]. It can be used to measure intermolecular and intramolecular interaction forces at high (pN) resolution by moving a small probe vertically (in relation to the sample), as well as scanning across the sample to observe topography, in addition to mechanotransduction in cells that are undergoing deformation [105].

AFM has been used to observe the anchoring strength of cholesterol in L_O and L_D lipid bilayer phases – cholesterol is known to be found more abundantly in L_O phase regions, and its increased anchoring strength reflects this [106].

Multifrequency AFM

This is a specialised AFM technique that can be used to effectively observe the mechanical properties of membranes in solution without using a contact mode of scanning. The cantilever is oscillated above the surface and operates in two eigenmodes of vibration. This has been used to view the arrangement of eye lens integral membrane protein aquaporin (AQP0) tetramers and the hydration structure of the membrane simultaneously (Figure 22), showing a clear lattice arrangement of tetramers that can be overlaid with the water affinity to show how they correlate [107].

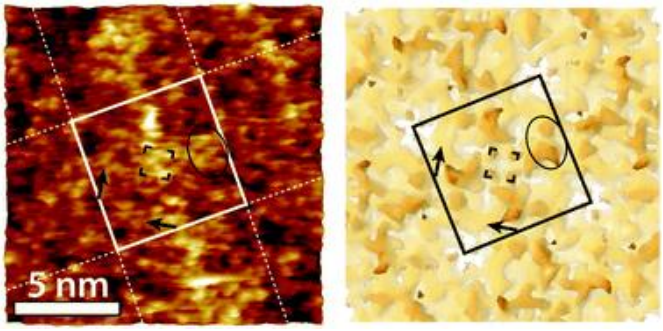

Figure 22: AQP0 forms tetramers arranged in diamond-shaped arrays in membranes, visible when imaged using multifrequency AFM. Taken from the paper by Ricci [107].

2.4.1.4 Super-Resolution Imaging

Traditional light microscopy methods are restricted in their resolution by the diffraction limit of light – the minimum distance to resolve between two points is limited to the Abbe limit, $d = \lambda/2.8$, by the wavelength of light used. There are methods that use smaller wavelengths to increase resolution beyond optical microscopy limits: X ray diffraction and electron microscopy for example, however there are now methods of going beyond the diffraction limit for whatever wavelength of light is being used; these are super-resolution methods [108].

Deconvolution theory can be used in confocal and widefield microscopy, by including a pattern or image in the incident light, and attempting to use the point scattering from the sample to reconstruct the pattern computationally (and therefore also resolve the sample features in more detail.) This is structured illumination microscopy (SIM). The data can become noisy as a texture will appear in the background of images, but particularly for known structures this is a useful method as it can be used in 3D or 2D imaging [109].

Localisation Microscopy allows features of known shapes to be localised to much greater precision than the resolution of the system would usually allow, taking multiple images with few fluorophores emitting light [110].

A variation of this technique, Bayesian analysis of Blinking and Bleaching (3B), allows the number of fluorophores to be increased per image and allows for overlap. It does this by utilising pre-determined likely behavioural modelling of fluorophores and treats the entire dataset as a number of fluorophores that may be emitting or not emitting light at any time of measurement. The dataset from one timepoint is also linked to the previous state of the system [111]. This modelling requires quite a long time to run and analyse the data because of this but the technique offers good spatial and temporal resolution for appropriate systems – for example in the observation of podosome formation and dissociation mechanics across a whole cell to resolution of 50 nm on a 4 s timescale. Podosomes are actin-rich structures

with a central core and ring structure surrounding of integrin-associated ring proteins (eg talin, vinculin) that bind to the membrane, associated with cellular migration, adhesion and extracellular matrix (ECM) degradation. They were predicted to cycle from forming to dissociation in 5-10 minutes – using the 3B method, the ring structures were made clearly visible [112].

Data analysis is key to super-resolution microscopy; this has given rise to tools like ThunderSTORM, that can assist with automation of raw data handling, post-processing and visualisation of data – ThunderSTORM itself is designed to work with Stochastic optical reconstruction microscopy (STORM) or photo activated localization microscopy (PALM), both methods that use sets of differing photoswitchable fluorophores activated sequentially and resolve in time to find the location of each point with high precision [113].

2.4.1.5 Correlative imaging

AFM is limited in that assumptions must be made based on topological and force spectroscopy imaging; essentially a 'stab in the dark' approach – using AFM in conjunction with other imaging methods like STORM or Total Internal Reflection Fluorescence Microscopy (TIRFM) can be used to gather correlating data for processes where prior assumptions cannot necessarily be applied to suit a singular method. As an example, TIRFM/ AFM; This has applications in looking at Anti-Microbial Peptide interactions with membranes; induced changes in membrane ordered/disordered state can be observed oh peptide binding and insertion, whilst simultaneously following molecular-scale changes in topography. Using fluorescent tagged peptide targets in model membranes the interactions can be observed by TIRFM as the membrane changes are tracked by AFM, giving insight into the orientation of the peptide and the dynamics of the role it plays in membrane restructuring [114].

2.4.2 Membrane Preparation & Merits of Model Membranes

The sheer complexity of components in membranes makes it very difficult, or even impossible, to do certain experiments using them alone – if more specific control of variables is needed, or to avoid unwanted additional interactions affecting results it is often better to use a model membrane system that mimics the complexity and physiochemical conditions as closely as possible, whilst retaining a greater degree of control over the composition and likely interactions. For the purposes of lipid-membrane or protein-membrane interaction observation, there are various types of model – which will produce the best results is dependent on what system is being mimicked [115]. It can also be beneficial to test membranes from living cells alongside model membranes, to see if predicted behaviour matches the model and therefore if any other factors are influencing results in the cell membranes.

Giant Unilamellar Vesicles (GUVs): These are large (size >1000 nm), single bilayer vesicles suspended in aqueous environment (Figure 23). Due to their surface curvature and unsupported nature they are useful for the mapping of phase boundaries of combined systems of saturated and unsaturated lipids with cholesterol; in particular the phase boundaries for different ratios of DOPC (1,2-dioleoyl-sn-glycero-3-phosphocholine), DPPC (1,2-di-d31-palmitoyl-sn-glycero-3-phosphocholine) and cholesterol at different temperatures have been mapped using this type of model [116].

They can also mimic the structure and formation of lipid rafts present in cells. Formation of GUVs is carried out by spreading a lipid mixture onto a platinum electrode in organic solvent to form multiple lipid layers, followed by dipping the electrodes into aqueous buffer and applying an electric field (alternating current as it is more efficient), typically around 2-3V. They can be prepared with gentle hydration, which creates electrostatic repulsion between bilayers and eventually results in GUV formation [117].

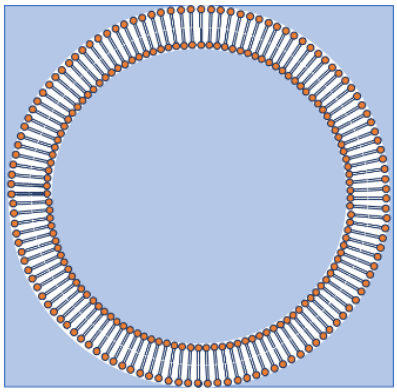

Figure 23: GUV and SUV structure. Small (<100 nm) and giant (>1000 nm) vesicles are approximately spherical shells formed from a single, continuous lipid bilayer.

Small Unilamellar Vesicles (SUV): These are structurally alike to GUVs but are smaller (<100 nm). They are useful for model membrane production as they can be introduced to a surface and burst relatively easily, producing a single layer of supported lipid bilayer.

Giant Plasma Membrane Vesicles (GPMVs): Vesicles formed of real cell membrane, usually chemically induced to bleb and separate off from the main cell, GPMVs are suitable models for observing cell membranes and proteins as closely as possible to their in vivo state; for example to observe the effect of lipid modifications on membrane proteins, as well as evaluation of the molecular composition and packing of cell membranes [115].

2.4.3 Types of artificial membrane

Supported Lipid Bilayers (SLBs): Consisting of membranes lying flat on a hydrophilic support such as mica or silica, with a very thin liquid layer between the support and

membrane (Figure 24). Easily accessible for viewing by optical microscopy as well as surface probing techniques like AFM. The supported nature of these models allows for greater flexibility with changing physical conditions without disrupting the membrane, for example to observe the sample with different buffers added in succession. These models are useful for evaluating membrane thicknesses and stability, such as effects of sphingolipid ceramides on membrane domain organisation [118]. It is possible to directly spin coat membranes onto substrate, but the most common way to prepare this type of model membrane is to burst/melt small vesicles (SUVs) onto a solid, hydrophilic substrate – the vesicles are adsorbed onto the surface, then ruptured and spread into the final flat bilayer formation.

Successful SLB formation is dependent on the properties of the support (roughness, surface charge, and chemical composition), the vesicles (size, charge, composition) and the surrounding aqueous environment. The inclusion of divalent ions is known to influence SLB formation, participating in charge screening to alter electrostatic interactions as well as more subtle interactions with surface and lipids. As a general trend, Calcium has been observed to promote vesicle adsorption, rupture and SLB formation. It is especially effective using mica supports, with mM concentrations sufficient to significantly aid SLB formation [119].

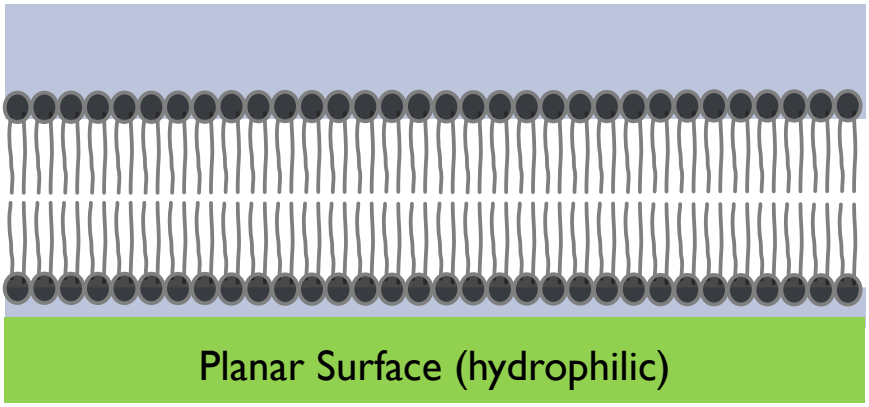

Figure 24: Supported Lipid Bilayer. On a hydrophilic support substrate, the hydrophobic tails of the lipids preferentially face away from the surface. The most favourable conformation is a bilayer of lipids, with the hydrophobic tails pointed into the centre.

Lipid Monolayers: single layers of phospholipids adhered to a support (Figure 25); similar to bilayers in that they are planar; quite far removed from physiological conditions in general.

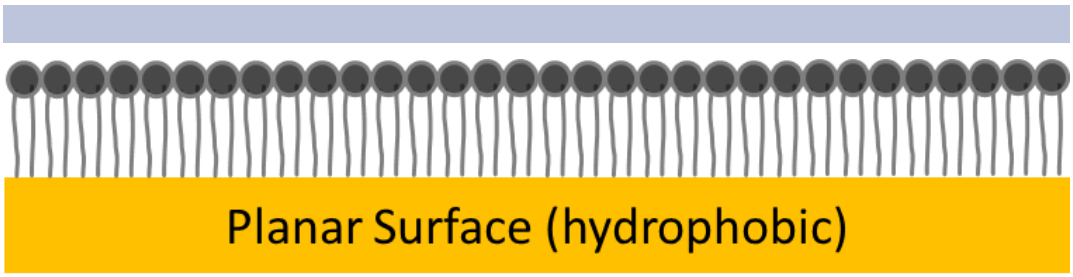

Figure 25: Supported Lipid Monolayer. The hydrophobic tails preferentially interact with the hydrophobic surface, making the formation of monolayers favourable.

2.5 Ongoing Research

The base of knowledge about the eye lens is ever-growing – a greater understanding of how the lens structure informs function and how this changes during ageing is being brought to bear in new medical research, but there is always more to understand.

Current medical research into the eye lens is seeking to find new forms of treatment for age-related cataract beyond the only current treatment, which is surgically replacing the lens with an artificial plastic lens. This surgery is expensive and carries risks of infections, inflammation and a night time halo effect in vision. In babies with congenital cataracts it is also dangerous, as the eye is still developing.

An alternative could be to remove cataractous lenses and either grow replacement lenses external to the body in some form of scaffold [120], or to leave the lens capsule as intact as possible and trigger development of a new lens in the patient from endogenous lens progenitor cells. The latter has been shown to regenerate some lens function in animals (Figure 26) and infant humans with congenital cataracts [121], but whether a similar approach would be effective for fully grown humans is unclear and surgery is still required for the procedure. This method also carries the risk of developing amblyopia, an impairment of vision caused by over-stimulation during the regenerative process.

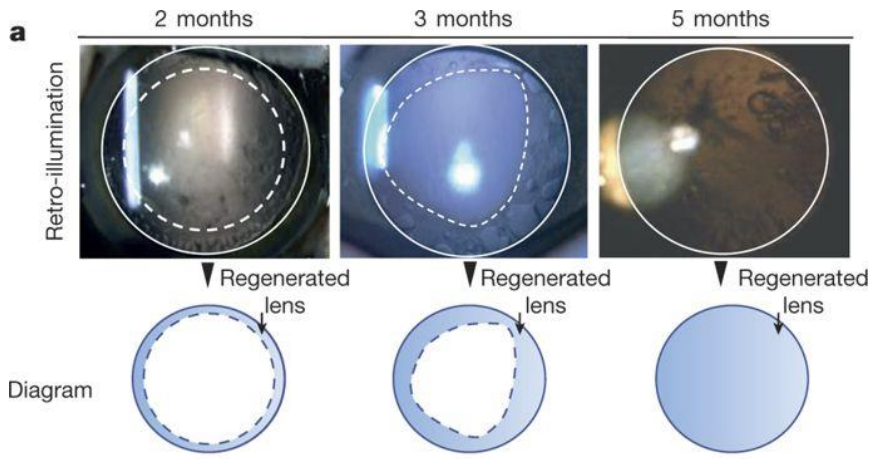

Figure 26: Lens regeneration in macaque models. Over the course of 5 months, lens progenitor cells in macaques was used to regenerate functional lens tissue after surgical lens removal. Figure adapted from the paper by Lin [121].

Non-surgical options to reverse cataract formation would be preferable if they could be developed – treatments that could be applied in the form of eye drops or a dietary supplement are an attractive prospect, but research thus far has not proved fruitful. Claims that application of some oxysterols such as lanosterol and 25-hydroxycholesterol to the eye could reverse cataract formation by binding to crystallin proteins have been recently debunked [122]. Although diets with suitable nutrient levels do seem to be beneficial to healthy lens ageing this does not ultimately prevent or treat cataracts [123].

For non-surgical treatments and prevention especially, a deeper understanding of how components of the lens behave and interact on different length scales is required – particularly, in light of the recent debunked claims that some oxysterols may reverse cataract formation, a specific knowledge of the effects of oxidised sterol levels increasing in the lens, from individual bilayer scale up to more complex interactions. This work aims to address part of this knowledge gap, by observing on a membrane-scale how oxysterol presence affects behaviour.

Chapter 3 Materials & Methods

3.1 Bovine Lens Membrane Extraction

Fresh adult bovine eyes were obtained from a local slaughterhouse. Membranes were isolated using an adapted version of the protocol by Kistler[124]. The lenses were removed and decapsulated, then hydrodissected in a low salt extraction buffer (10 mM Na_3PO_4, 100 mM NaCl, 5 mM EDTA, pH 7.4) to separate defined cortex and nuclear (residual lens) fractions. These lens fractions were individually dounce homogenised in an ice bath. The homogenates

were then centrifuged at 15000 rpm for 15 minutes at 4 ^{0}C. The supernatant, containing the water-soluble fraction, was discarded and the membrane-enriched pellet was retained. The pellet was then resuspended in the same buffer, and the process of Dounce homogenisation, centrifugation and pellet resuspension was repeated using the following buffers;

10 mM Na_3PO_4, 1.5 M KCl, 5 mM EDTA, pH 7.4

10 mM Na_3PO_4, 100 mM NaCl, 5 mM EDTA, pH 7.4 (repeat initial buffer)

10 mM Ammonium bicarbonate, 1 mM EDTA pH 7.4

10 mM Na_3PO_4, 8 M Urea, 5 mM EDTA

Once resuspended and homogenised in the 8 M Urea buffer the samples were kept on spin for 20 minutes, then washed once more in the extraction buffer and stored at 4 ^{0}C.

This preparation leaves some transmembrane proteins still present in the lipid membrane.

3.2 Substrate Preparation

Mica disks were used for the SLB solid supports, as the material properties are well-documented, and the positive effect of divalent $CaCl_2$ in the buffer used on SLB formation is particularly effective on mica[119] .

Mica disks were attached to cleaned microscope slides using epoxy resin similar to the procedure outlined by Miller [125].

A dot of freshly-mixed epoxy was placed onto a clean glass slide and a mica disc pressed on top. Care was taken to ensure no excess of epoxy was left around the edges of the substrate (either from excessive force when pressing on the disk, or an excess of material) to avoid direct exposure to air and potential contamination. The epoxy was left to cure fully prior to use.

Immediately before addition of membrane solution, adhesive tape was pressed firmly over the disc and smoothly peeled off so that removed material is visible on the tape. This was repeated 2-3 times to ensure the entire surface is freshly-cleaved and as smooth as possible.

3.3 Membrane Sample Preparation

3.3.1 Models

3.3.1.1 Composition

Initially three different membrane compositions were selected to mimic the lipid and cholesterol content of bovine LFC membranes [37]. For cholesterol extraction experiments, the cholesterol content was replaced with Thiocholesterol (Figure 27). This cholesterol

analogue has an exposed thiol group at one extremity in order to facilitate covalent bonding to functionalised Au-coated AFM tips.

- DOPC 40% + 60% Cholesterol
  Simplest membrane composition with high cholesterol content to mimic lens nucleus levels
- DOPC 16.5%, DPPC 38.5% + 45% Cholesterol
  Stiffer DOPC: DPPC membrane with high cholesterol content to mimic lens cortex levels – this model was only used in earlier experiments due to time constraints.
- SM 22%, DOPE 33%, DPPC 25% + 20% Cholesterol
  Low cholesterol concentration for ease of membrane formation; focus on mimicking lens lipid composition including sphingomyelin.

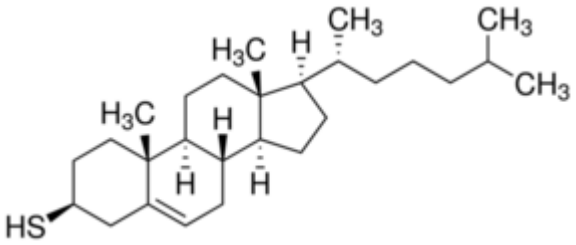

Figure 27: Thiocholesterol – Structurally similar to Cholesterol, but with a thiol group replacing the hydroxyl group at one end of the molecule. Structural image taken from Sigma Aldrich [126].

3.3.1.2 Preparation

Lipid Stocks

Stock lipid solutions were made up in chloroform to minimise oxidation, in relatively large quantities compared to those needed for single experiments – this allowed for multiple experiments to be carried out using each stock solution, minimising variation in lipid content between preparations. Stock solutions were stored in glass vials with Teflon-lined lids in a freezer when not in use.

Stock 1 prepared at 10 mg/ml

Stock 2 prepared at 1 mg/ml

Stock 3 prepared at 2 mg/ml

For FRAP experiments, separate model stock solutions were prepared as above, but with a rhodamine tag included at 0.5% concentration.

Sample from Stock

Prior to use the desired quantity of stock was desiccated, resuspended in buffer and sonicated until the sample became clear, indicating the correct SUV size had been reached.

To form SLBs, 200 µl of the lipid sample (0.5 µg/ml) and 75 µl 7-ketocholesterol (1.2 µg/ml in ethanol EtOH) for ketocholesterol samples was pipetted onto the freshly cleaved mica disc, and buffer (2 mM $CaCl_2$, 150 mM KCl, 10 mM Trizma base, pH 7.5) was added to fill the ring well to 1.5 ml. These samples were then covered and incubated for 1 hour at 60 ^{0}C, then cooled over 12 hours to 25 ^{0}C, to ensure successful bilayer formation.

After incubation, samples were gently rinsed ten times with 500 µl buffer before being used for imaging.

3.3.2 Native Membranes

3.3.2.1 Composition

Lens fractions from the Outer Cortex (OC) and Inner Nucleus (IN) were selected for testing, in order to cover the full range of membrane variation across the lens.

3.3.2.2 Preparation

To prepare the native lens membrane samples a similar approach was taken to that taken by Buzhynskyy and Ricci [70, 107]. 10 µL of the selected lens membrane solution was dissolved in 50 µl of adsorption buffer (25 mM $CaCl_2$, 150 mM KCl, 10 mM Trizma, pH 7.5) and incubated for 10 minutes on a freshly-cleaved mica disc. For ketocholesterol test samples, 3.75 µl of ketocholesterol in EtOH (1.2 mg/ml) was added for the incubation stage. More buffer was then added to 1.5 mL, and the samples were gently rinsed ten times with 500 µl buffer before being used for imaging.

The samples were tested with the incubation method used for the topography/force mapping experiments prior to rinsing and without incubation. All chemicals used to produce the buffers were purchased from Sigma-Aldrich (Sigma- Aldrich, St. Louis, Missouri, USA) and dissolved into ultrapure water (Milli-Q, 18.2 OM, o5 ppm organics, Merck-Millipore, Billerica,)

Ketocholesterol Samples

Adding ketocholesterol in chloroform after heated incubation was not viable, and native membranes were always kept in buffer so ketocholesterol was added in EtOH – noting the effects of EtOH on bilayers [127]– but the proportion was kept to a minimum and the sample rinsing before imaging should have removed most of the EtOH in the buffer solution.

3.4 Fluorescence Recovery After Photobleaching (FRAP)

Once prepared, the rhodamine-tagged model membrane samples were imaged at 20 X with a Nikon confocal microscope

Three areas from each sample were selected for imaging. A pre-bleach image of each area was taken, and then a small rectangle was bleached 10 times (to minimise remaining fluorescence in that area) immediately before beginning image sequencing. Each area was imaged at 5 second intervals over a period of 10 minutes (Figure 28).

A visual comparison of start and end images for each experiment was made to check if recovery was visible before further analysis, to confirm if a membrane was present.

Figure 28: Fluorescence Recovery After Photobleaching (FRAP): A small rectangular area is selected for bleaching. Immediately after bleaching, there are no working fluorophores in the area so it appears a black. Recovery of fluorescence in the bleached area indicates the presence of a fluid membrane, as fluorophores are able to diffuse in.

Images were converted into TIFF stacks and analysed using the simFRAP plugin [128] in ImageJ. Recovery of fluorescence in the bleached area was used to obtain a diffusion coefficient for the lipids in each sample, allowing 1000 iterations per stack to prevent crashing.

3.5 Atomic Force Microscopy (AFM)

All AFM data was collected using a JPK NanoWizard® AFM, with the sample and cantilever/tip fully immersed in the imaging solution.

3.5.1.1 Tip Preparation

General Procedure

For Topography, Phase and Force mapping a silicon nitride cantilever with a spring constant k ~ 0.76 N/m was used (RC800 PSA Olympus, Tokyo, Japan).

Prior to use, the tips were cleaned by soaking in isopropanol for 30 mins, followed by ultrapure water for 30 mins. Tips that had been used previously and required additional cleaning were first soaked in acetone for 10 mins to remove contaminants.

Once loaded into the cantilever holder, a drop (~20 µl) of imaging buffer was applied to pre-wet the cantilever, and to inhibit bubble formation when being immersed in the sample buffer upon approach.

Functionalisation for thiocholesterol extraction

A gold back-coated silicon nitride cantilever with spring constant k ~ 0.09 N/m was used (TR400 PB Olympus, Tokyo, Japan).

The cantilever was first immersed in acetone for 10 minutes, dried on lint-free tissue, then exposed to UV light for 20 minutes to leave exposed OH- groups on the surface (with care taken not to over-expose and cause excessive tip blunting) before being immersed in EtOH for 1 hour. It was then transferred to a bath of ultrapure water for 30 minutes before loading, pre-wetting and use.

Cantilever Calibration

In order to obtain reliable force measurement, it is necessary to first calibrate the spring constant of a cantilever. This is because there can be significant variations from cantilever to cantilever due to the manufacturing process. To do so, the laser was positioned near the tip end of the cantilever whilst fully immersed in imaging buffer and then aligned. In liquid, the spring constant of the cantilever is lower than in air due to damping, so an estimated spring constant value given by the cantilever geometry alone would have been insufficient.

Thermal noise fluctuations were measured, and the cantilever is treated as a harmonic oscillator to find fundamental eigenmode frequency (automated with correction factors as it is not perfectly harmonic).

Contact mode calibration was used to convert measured deflection on the photodetector (V) to the real deflection of the cantilever (nm). A deflection vs distance curve was taken, and the deflection calibrated by imposing the slope of the curve in the linear region of deflection to be unity. This would preferably be done last so as to not damage the tip, and preferably on a hard, flat surface.

3.5.2 Data Collection & Analysis

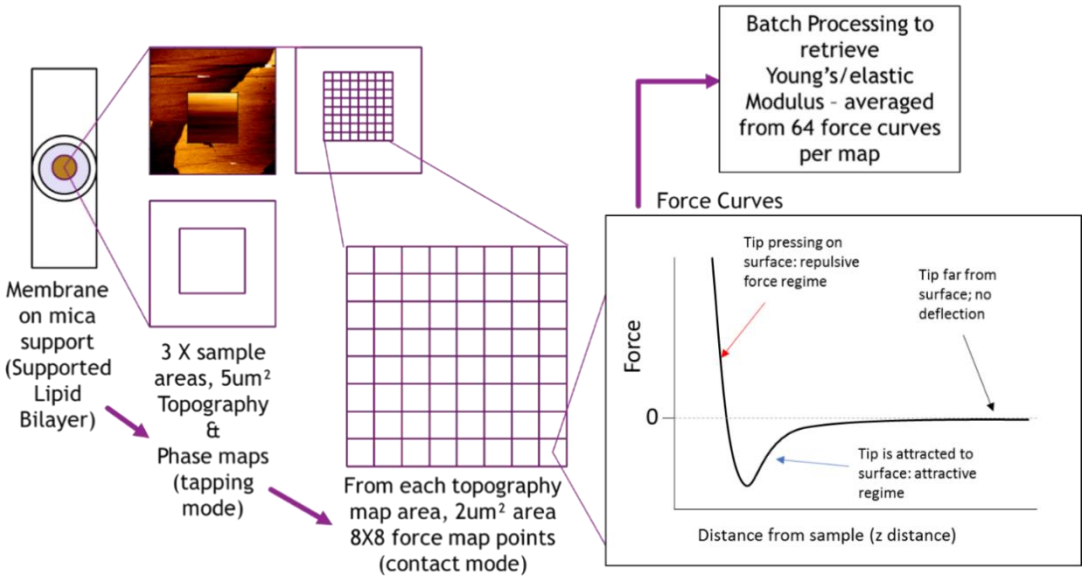

Figure 29: Topography, phase and stiffness data collection procedure: For each sample, 3 areas of 5 μm² were selected randomly for topography & phase imaging. 2 maps were taken per location to check consistency. Within each selected area, a 2 μm² square was used to collect an 8X8 point force map.

3.5.2.1 Topography & Phase Mapping

For each imaging area selected (Figure 29), topography maps were created using the 'tapping' or intermittent contact mode, where the cantilever is oscillated at a specific frequency close to resonance and maintained at a set oscillation amplitude as it moves across the sample (Figure 30).

This is done by adjusting the piezo height – as the sample scans over the surface, the amplitude will be damped if sample height increases, and a feedback loop applies voltage to the piezo to move the cantilever vertically and restore the set amplitude. From these corrections topographic information is obtained, and the phase lag between the drive signal and cantilever is also measured.

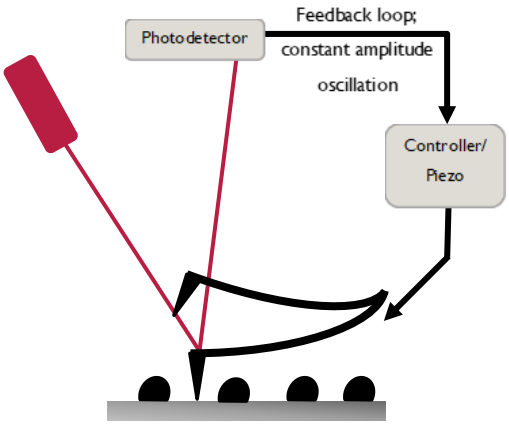

Figure 30: Intermittent contact or tapping mode atomic force microscopy. The cantilever is oscillated at a set amplitude close to resonance frequency as it moves across the sample, collecting topographic and phase information simultaneously.

This mode of imaging was selected as it is gentle enough to soft surfaces without causing damage, and lateral drag isn't an issue as with contact mode. A relatively high setpoint was kept, to maintain a low imaging force whilst still being able to accurately map the surface.

3.5.2.2 Force Mapping & Young's Modulus

After topography mapping, a 2 μm^2 region from each area was force mapped using contact mode AFM in an 8 by 8 square. (Figure 31).

Parameters were set as follows:

- Relative Setpoint: 0.5 nN,
- Z length: 0.2 µm,
- Extend Speed: 0.2 µm/s

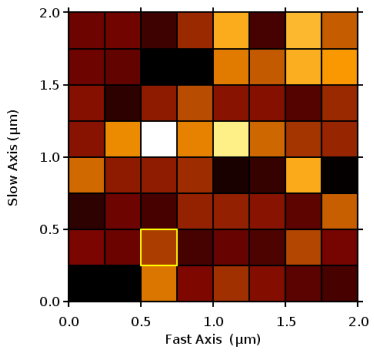

Figure 31: Example of an 8 X 8 force map measured with atomic force microscopy. Each square represents a point measured; lighter colours indicate higher Young's moduli.

Data Processing

A batch process using the JPK data processing software was set up to extract Young's Moduli from the force map curves rapidly and consistently. This process takes each force curve and the cantilever spring constant and sensitivity determined during the calibration stage of setup (see above). It subtracts the baseline, corrects for tip bending and then fits the data to determine a value for the Young's Modulus (stiffness) of the membrane.

This fitting was done using the Hertz-Sneddon model, which combines estimates for spherical and conical indentor geometries (Figure 32). A more complex brush model was not deemed necessary in this case as only simple membranes and not whole cells were being tested [129].

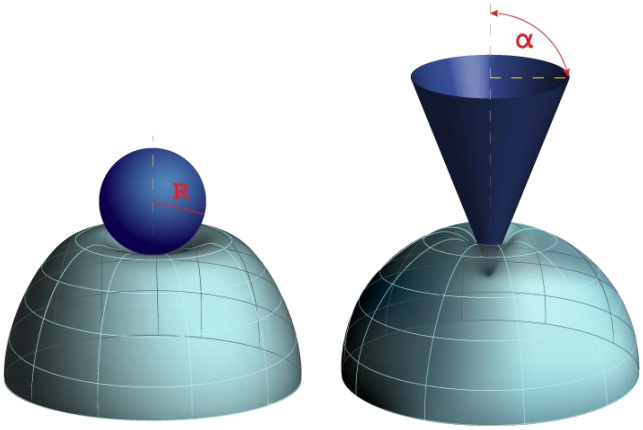

$$(F)^{2/3} = \left(\frac{4}{3}\frac{E}{(1-\upsilon^2)}\sqrt{R}\right)^{2/3}\delta \qquad (F)^{1/2} = \left(\frac{2}{\pi}\frac{E}{(1-\upsilon^2)}\tan(\alpha)\right)^{1/2}\delta$$

Figure 32: The Hertz and Sneddon models for spherical and conical indentors. These use the force (F) from the force curve, the indentation (δ), the Poisson's ratio (ν) of the material and the radius or half-angle (spherical or conical) of the indentor (R or α), in order to compute the Young's modulus (E) and adhesion of samples. Adapted from the Bruker website [130].

For each preparation an average of the Young's Modulus values was calculated, and these averages were compared to observe the percentage change in YM/ stiffness of the membrane.

3.5.2.3 Cholesterol Binding Affinity

Thiocholesterol Extraction

To measure the force required to extract single cholesterol molecules from the model membranes, the functionalised cantilever is brought down to the surface and held in position to allow time for thiocholesterol to bind. The tip is then retracted, extracting the tethered thiocholesterol molecule and recording the associated forces simultaneously. Single or

multiple step events in the extraction curves can be present due to the potential for multiple binding events.

16 X 16 points are measured in a 2 μm^2 area for each map. Three areas were mapped per sample, and repeat samples measured for each model type. At each point, the cantilever approaches and is held at the surface for 1 s before being pulled back

Parameters were set as follows:

- Relative Setpoint: 0.5 nN,
- Z length: 0.3 μm,
- Extend Speed: 0.1 μm/s
- Extend delay: 1.0 s

Data Processing

Extraction curves were taken and processed using the JPK SPM data processing software. A similar batch process to the force mapping analysis was created, which follows these steps;

- Baseline subtraction
- Uses tip calibration values to input cantilever Spring Constant and Sensitivity values
- Corrects for cantilever bending
  Step fitting & parameters

Chapter 4 Results and Discussion

The primary objective of this research project was to determine how the biophysical properties of eye lens membranes are affected by raised levels of 7-ketocholesterol, an oxysterol which accumulates during ageing and in cataractous lens membranes. The data indicate significant changes to the lipid lateral diffusion rate, single lipid anchoring strength and membrane stiffness in lens membrane models. This reflects concurrent changes to membrane stiffness in native lens membranes when 7-ketocholesterol is present.

4.1 FRAP - Lateral diffusion characteristics of lipid model bilayers

Sample	*Start Frame (t=0 minutes)*	*End Frame (t=10 minutes)*
A: DOPC	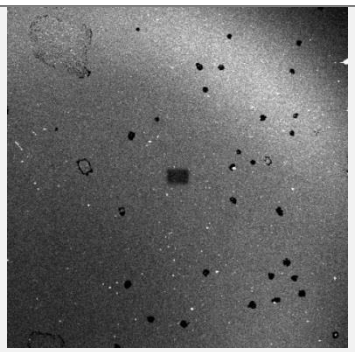	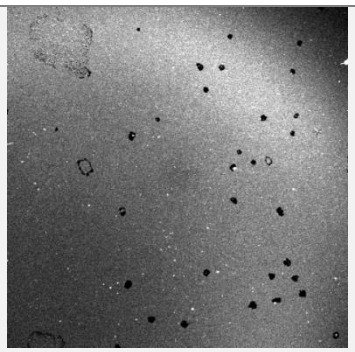
B: DOPC + 7-ketocholesterol	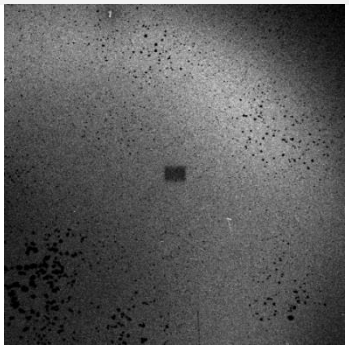	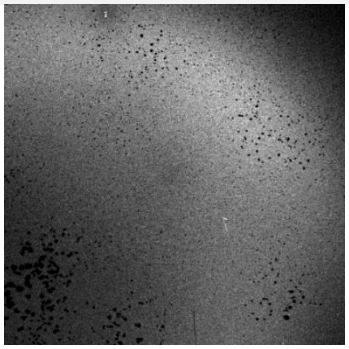
C: SM:DOPE:DPPC	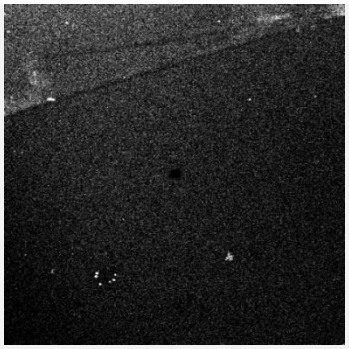	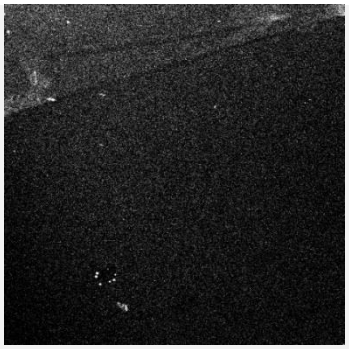

D: SM:DOPE:DPPC + 7-ketocholesterol

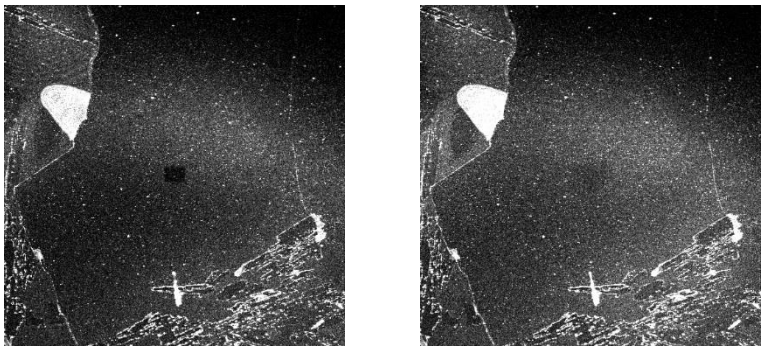

Figure 33: FRAP images demonstrating the recovery of membrane bilayers

The final preparation procedure was shown to successfully produce dynamic lipid bilayers – visible by the fluorescence recovery of the bleached patch as the lipids move within the bilayer. (Figure 33)

Visually most bilayers not incubated with 7-ketocholesterol appear uniform in fluorescence distribution both before bleaching and after recovery, with clear, sharp-edged dark areas that indicate where the mica has cleaved unevenly (Figure 33). The 7-ketocholesterol incubated samples are less consistent, with some showing clearly divided areas varying in brightness and some dark areas that do not resemble the mica defects.

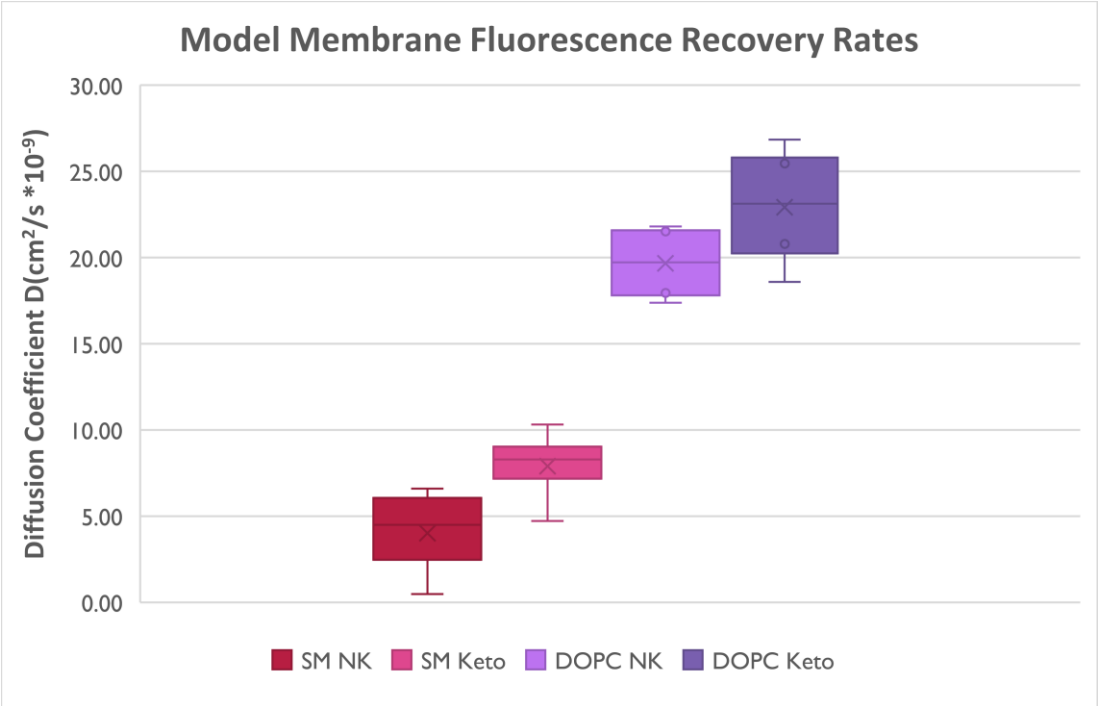

Figure 34: Fluorescence recovery rate after photobleaching for model membranes increases slightly on average with 7-ketocholesterol present. This effect is observed in both sphingomyelin containing (SM) and DOPC: cholesterol bilayers, where NK indicates a sample without 7-ketocholesterol present. The increase in diffusion coefficient corresponds to an increase in bilayer fluidity when 7-ketocholesterol is present in the membrane.

As well as establishing that fluorescence recovery is occurring to confirm the presence of lipid bilayers, the processed data gives an indication of the lateral diffusion characteristics of the bilayers and how they are affected by the presence of 7-ketocholesterol (Figure 34).

Cholesterol is known to control fluidity in the membranes of the eye lens, in order to keep a similar degree of lipid ordering throughout the cortical and nuclear regions [29]. This is reliant on the stiff, flat steroid moiety of the planar α-face, which allows it to intercalate between lipid hydrocarbon tails, inducing more lipids to lie in the trans configuration, packing tighter and maximising attractive Van der Waal's forces to condense and stiffen the membrane overall [26]. 7-ketocholesterol has an additional double bonded oxygen interrupting the planar α-face, so it is predicted to be less (if at all) effective at membrane ordering than pure cholesterol, similar to how the cholesterol precursor lanosterol, with included methyl groups, cannot replace cholesterol functioning [27].

The FRAP data collected shows a significant increase in the membrane recovery coefficient D upon the addition of 7-ketocholesterol to the lipid bilayers, indicating an increase in the lateral lipid diffusion rate, and therefore a decrease in membrane stiffness. These results agree with the hypothesis that the normal function of cholesterol in membranes - to induce tighter lipid packing and therefore increase stiffness [32]- is being disrupted by the inclusion of the oxysterol.

The biological implications of this could involve the alteration of protein membrane interactions, for example in the arrangement of trapped and boundary lipids around the AQP0 tight junction and Connexin gap junction clusters, the structure of which is key to their function. These junctional domains are thought to usually be in more ordered phases, so diminishing cholesterol's ordering ability in these domains could lead to the disruption of cell adhesion and transport of metabolites and water. This would agree with the findings of Girão [131], where the presence of 7-ketocholesterol induced an increase of Connexin 43 in gap junction plaques. This increased intercellular exchange of water and metabolites and could have potentially led to the interruption of tightly controlled processes, such as LFC differentiation, that are required for maintaining lens transparency.

The SM containing bilayers have a lower diffusion coefficient than the less complex DOPC, indicating that they are initially stiffer. This is expected, despite them having a lower cholesterol content, because of the higher overall hydrocarbon tail chain order present in the SM bilayer and the increased variety of lipids present. Though initially stiffer, SM-containing bilayers are also more strongly affected by the inclusion of 7-ketocholesterol, with the average mean change being over four times greater than for DOPC: cholesterol bilayers [31].

The percentage median change to the diffusion coefficient was significantly greater in the SM-containing bilayer (Table 3), although the exact value of the change is quite similar.

It should be taken into account for the DOPC bilayer that cholesterol in lipid membranes increases stiffness up to a certain percentage, and then decreases it if more cholesterol is added above that by the formation of cholesterol bilayer domains [132]. In the DOPC bilayers the percentage of cholesterol is high enough, in theory, to enable the formation of these domains.

These observations correlate with the observed function of cholesterol in decreasing Dc in DOPC bilayers by Ladha [99]; disruption of Cholesterol weakens the ability to structure the bilayer, and 7-ketocholesterol is observed to have this effect.

Table 3: Diffusion coefficient medians of bilayers with (keto) and without (NK) 7-ketocholesterol included in the membrane. In both bilayer compositions tested the diffusion coefficient increases, indicating that the bilayers are more fluid. This effect is more evident in the sphingomyelin-containing (SM) bilayers.

Medians

	NK	Keto	% Change
SM	4.498	8.284	84.17%
DOPC	19.725	23.125	17.24%

4.2 Topography and Phase - AFM

4.2.1.1 Model membranes – topography and phase

Model	Topography	Phase
A: DOPC	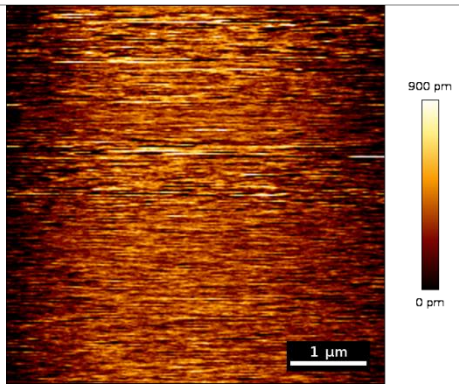	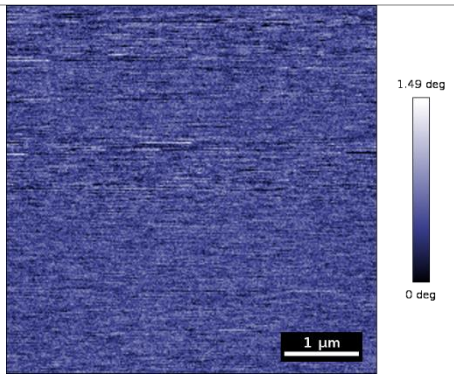

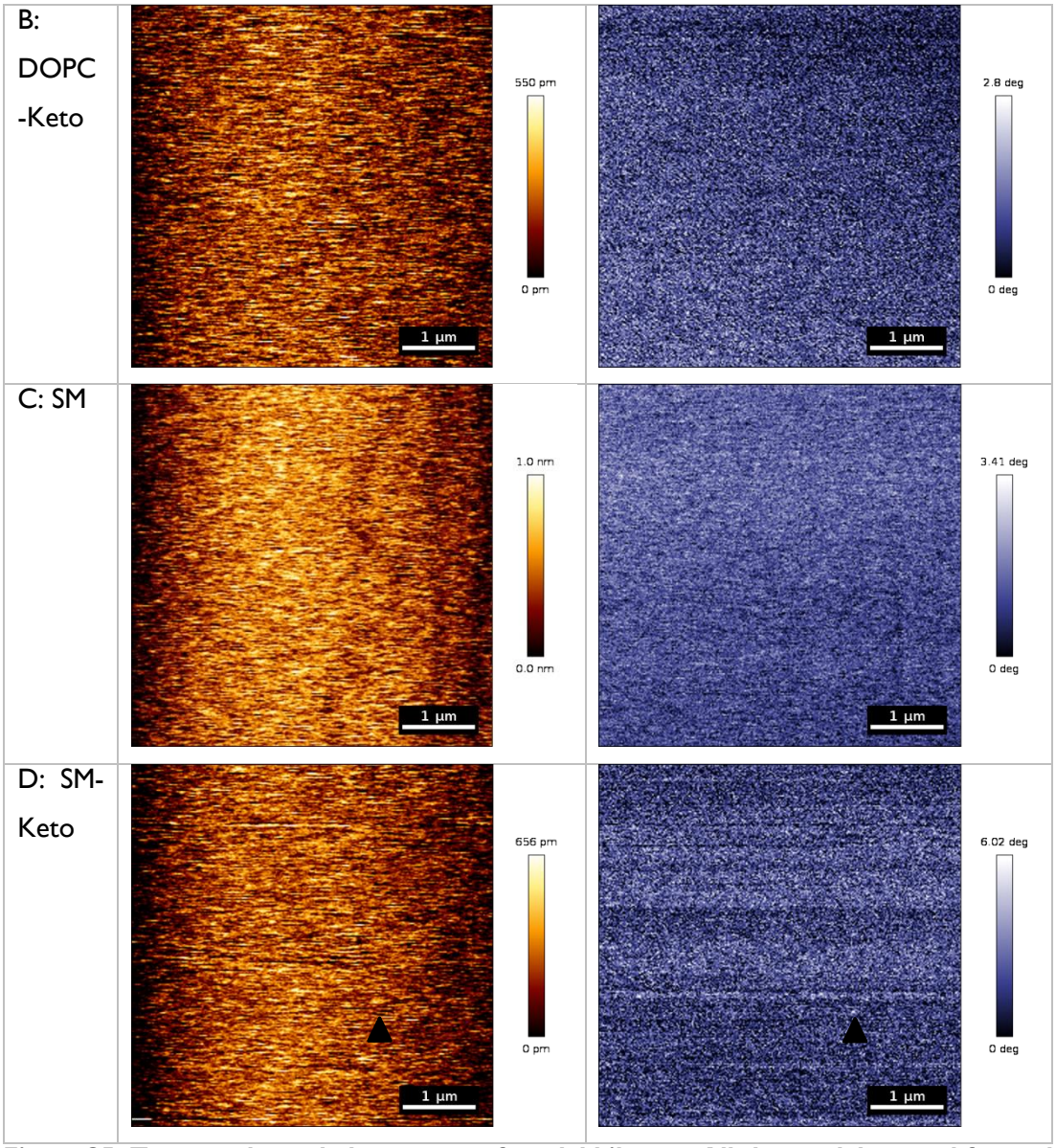

Figure 35: Topography and phase maps of model bilayers. All the models tested formed continuous bilayers with no large-scale phase separation. In some samples there were small 'dimples' (see pointers in D) visible in topography and phase images, raised around 0.5 µm from the bilayer. These may be small gel phase domains, and most frequently appeared in DOPC: DPPC: Cholesterol bilayers which were not further investigated here.

As the model membranes in these experiments do not contain lens-specific proteins, they cannot be expected to form structured arrays or domains that are dependent on the presence of these proteins, as you would expect to find in the eye lens.

The topography of all models tested was consistent with continuous lipid bilayers, although in some samples holes were found in the membrane, visible as very flat areas dropped approximately 5 µm below the main surface. The bilayers were largely uniform, with no large-scale phase separation apparent (Figure 35).

In some samples there were small raised 'dimples' visible on the surface. These primarily appeared on the DOPC: DPPC: cholesterol bilayers and could in theory be very small gel-phase raft domains, but are more likely to be vesicle debris – the distinction could not be made without further study, for example to test if their formation and stability are temperature-dependant; gel-phase nanodomains may disperse back into the bulk lipid with relatively small increases in temperature.

4.2.1.2 Native Lens Membranes

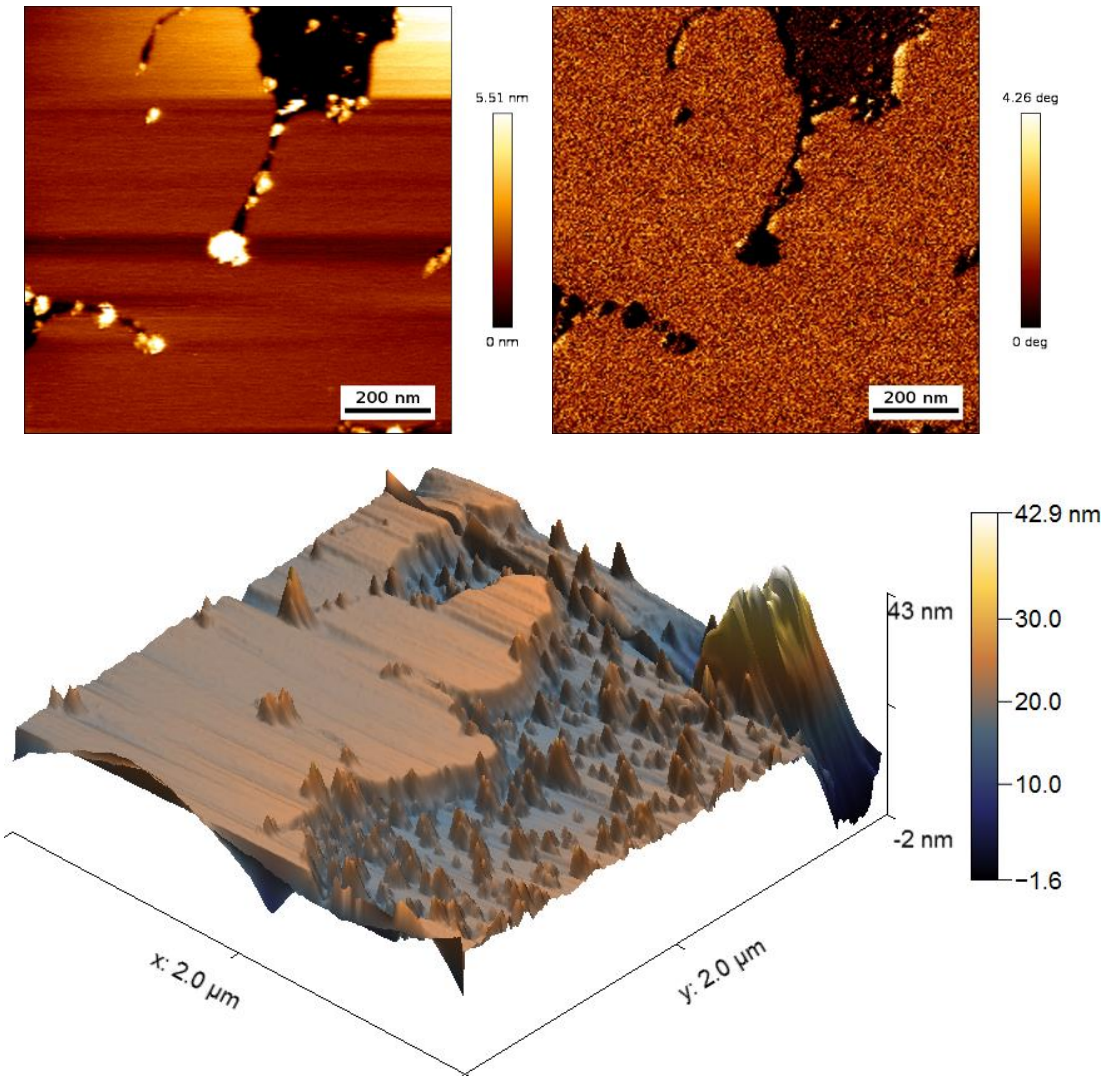

Figure 36: Outer cortex topography and phase images. The native lens membranes from outer cortex extracts formed near-continuous bilayers with no large-scale phase seperation visible. There were irregular, high peaks up to tens of nanometres above the surface that are likely aggregated proteins from the preparation steps.

The native membranes either formed as near-continuous bilayers or as patches on the substrate (Figure 36), with a characteristic height of about 5 µm. The inner nuclear membrane samples formed fewer and smaller discontinuous patches (Figure 37) but were otherwise

visually similar to the outer cortex membranes. The patches or continuous membrane sections were relatively flat, with no apparent large-scale phase separation, - No detectable areas of cholesterol bilayer or protein-associated lipid domains were visible. There were also irregularly positioned protrusions that were mostly far above the height of the bilayer, likely to be protein aggregates.

At the resolution allowed by this AFM, greater detail of the membrane surface could not be resolved, so the arrangement of structural proteins remaining within the membranes could not be observed if present.

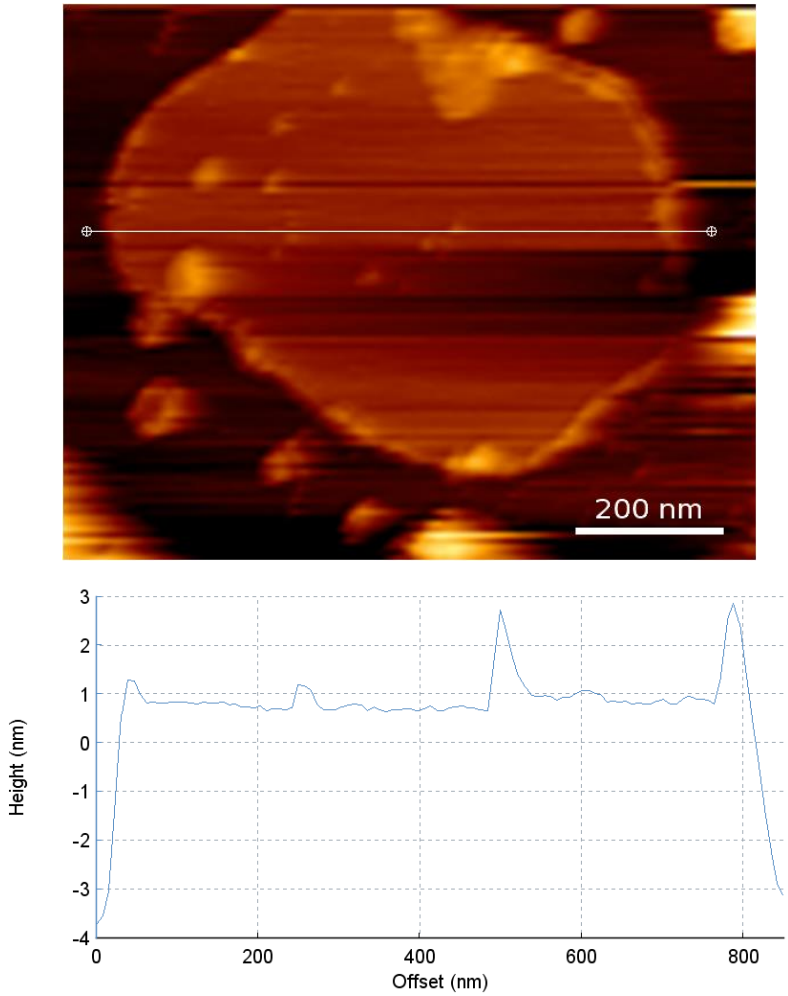

Figure 37: Inner nucleus patch topography and cross-section. The inner nuclear membrane fractions formed patches less readily than the outer cortex, with smaller, discontinuous patches and more irregular peaks forming that made the samples very difficult to image.

4.3 Force Mapping/Stiffness - AFM

Membrane Model/Fraction	Average Young's Modulus (untreated)/MPa	Average Young's Modulus (7-ketocholesterol)/MPa	Percentage change
DOPC:Cholesterol (set 1)	33.99	20.47	-39.8%
DOPC:Cholesterol (set 2)	20.78	10.49	-49.6%
DOPC:Cholesterol (set 3)	32.61	21.84	-33.04%
SM (set 1)	30.75	10.38	-66.2%
SM (set 2)	13.03	5.13	-60.65%
SM (set 3)	28.54	2.61	-90.85%
Inner Nucleus	10.67	8.57	-19.7%
Outer Cortex	37.09	16.11	-56.6%

Table 4: Average Young's Modulus Changes with ketocholesterol treatment. The average Young's modulus decreased for all membrane compositions tested, showing a decrease in stiffness when 7-ketocholesterol is included in the membrane. Sphingomyelin (SM) containing bilayers were the most affected.

A decrease in Young's modulus is observed in all model and native membranes (Table 4), constituting a decrease in membrane stiffness when incubated with biologically-relevant levels of 7-ketocholesterol. For DOPC: Cholesterol bilayers the average percentage change in the Young's Modulus was -40.81% and for SM bilayers it was -72.57%.

It is notable that similar percentage decreases in membrane stiffness were observed for the repeats of each model for the most part; as exact calibration values and conditions (for example tip shape, temperature, membrane stacks, dust) are not necessarily conserved between repeats there can appear to be quite a large difference in exact values measured for experimental repeats. The native membranes are particularly difficult to test, due to the presence of protein aggregates and the smaller average size of uniform membrane patches.

This decrease in stiffness will mean that eye lens membranes containing higher levels of 7-ketocholesterol will deform more easily when placed under physical strain – This is likely to have an impact on how strongly proteins can bind to the membranes and therefore the organisation of integral membrane proteins, including the important junctional proteins connexin and AQP0. When considered on the intercellular scale, malformation of junctional domains formed by these proteins affect cell adhesion, metabolite and water transport within

the lens, and their interaction with the membranes is crucial to function. A decrease in junctional effectiveness is observed during ageing and in cataractous lenses.

This is interesting in that the model containing a higher proportion of cholesterol was less affected by the inclusion of 7-ketocholesterol – this is likely due to the lipid content of the membrane, as cholesterol is known to preferentially associate with sphingolipids within membranes [26].

For future experiments a spherical indentor could be used to improve the fitting process.

Whilst not an issue for singular sets of experiments as the calibration for a single tip is retained for all measurements, it would be advantageous for future experiments to be able to increase accuracy and reproducibility without having to compare sets separately. This could be done by employing the Standardized Nanomechanical Atomic Force Microscopy Procedure (SNAP) developd by Schillers [133]. This procedure reduces the inaccuracies introduced during cantilever calibration through the use of a vibrometer to calculate deflection sensitivity values, allowing for more consistent measurements of the Young's Moduli for soft surfaces.

4.3.1 Force spectroscopy: measurement of adhesion

4.3.1.1 DOPC bilayers

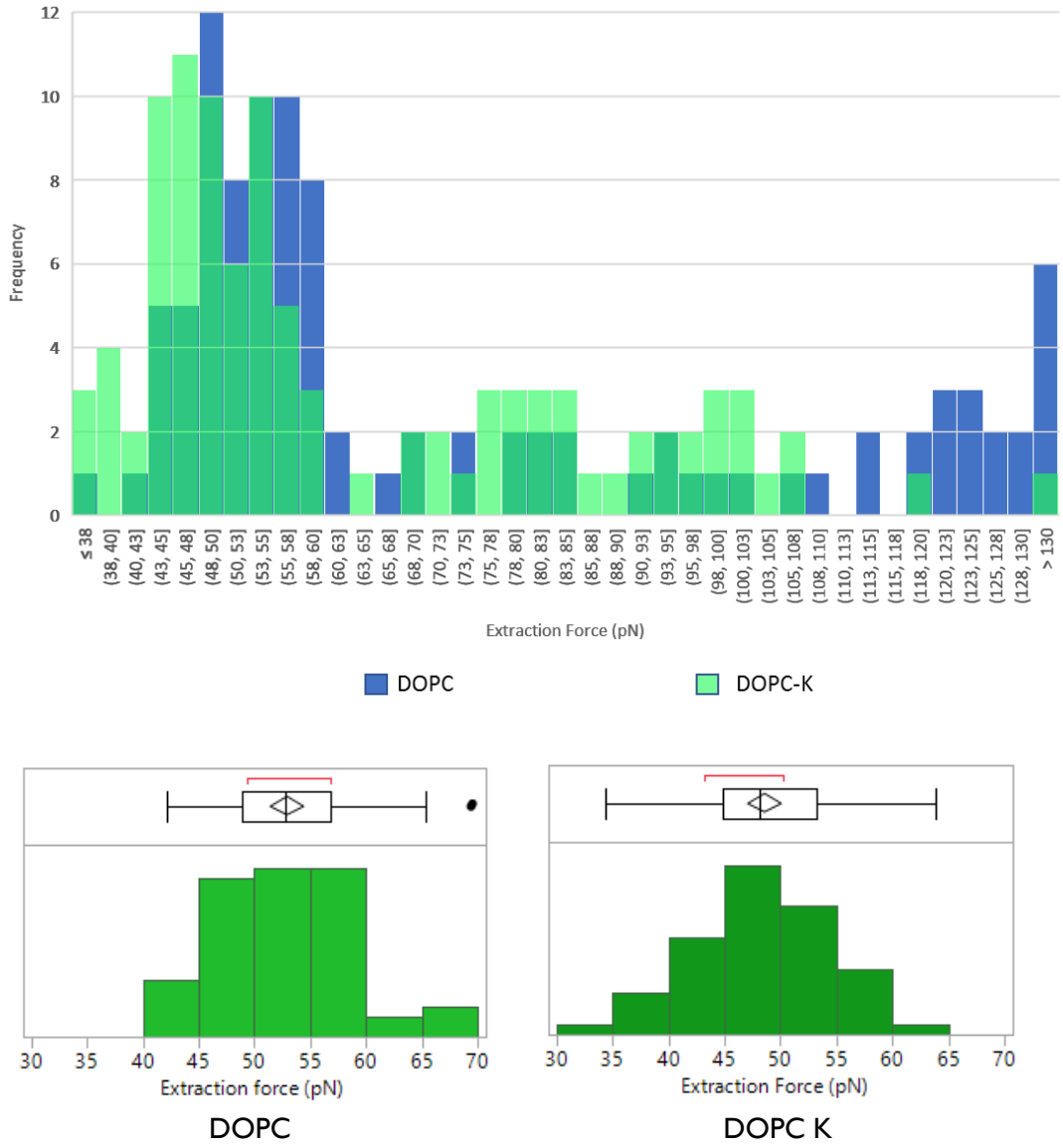

Figure 38: DOPC: Cholesterol bilayer comparative extraction forces. Top: Histogram of recorded extraction forces for membranes without (DOPC, blue) and with (DOPC-K, green) 7-ketocholesterol present, including overlap in a darker shade. The first peak that appears corresponds to the force required to pull a single thiocholesterol molecule from the membrane, latter peaks to multiple extraction events. This peak is shifted lower in ketocholesterol-containing samples, indicating that it is easier to pull thiocholesterol from these. Bottom: Simplified comparative histograms of values close to the first peak, showing that there is a decrease in the average force required for a single extraction event.

There is an initial clear peak in both datasets (Figure 38, top), likely to represent a single cholesterol extraction event, for the DOPC bilayer. The peak is shifted lower with the

inclusion of 7-ketocholesterol, shown simplified above (Figure 38, bottom). Analysis of the data from around the peak shows a drop in the mean extraction force required to extract thiocholesterol from the membrane, from 70.49pN to 60.81pN (Table 5).

Table 5: Single thiocholesterol extraction force data for DOPC bilayer. The inclusion of ketocholesterol (DOPC K samples) correlates with a drop in the extraction force for thiocholesterol, indicating that it is not held in the membrane as strongly.

Extraction Force (pN)

		DOPC	DOPC K
	Mean	70.49	60.81
	Standard Deviation	28.50	19.58
75.00%	quartile	88.08	78.10
50.00%	median	56.73	53.10
25.00%	quartile	50.00	46.16

4.3.1.2 Sphingomyelin containing bilayers

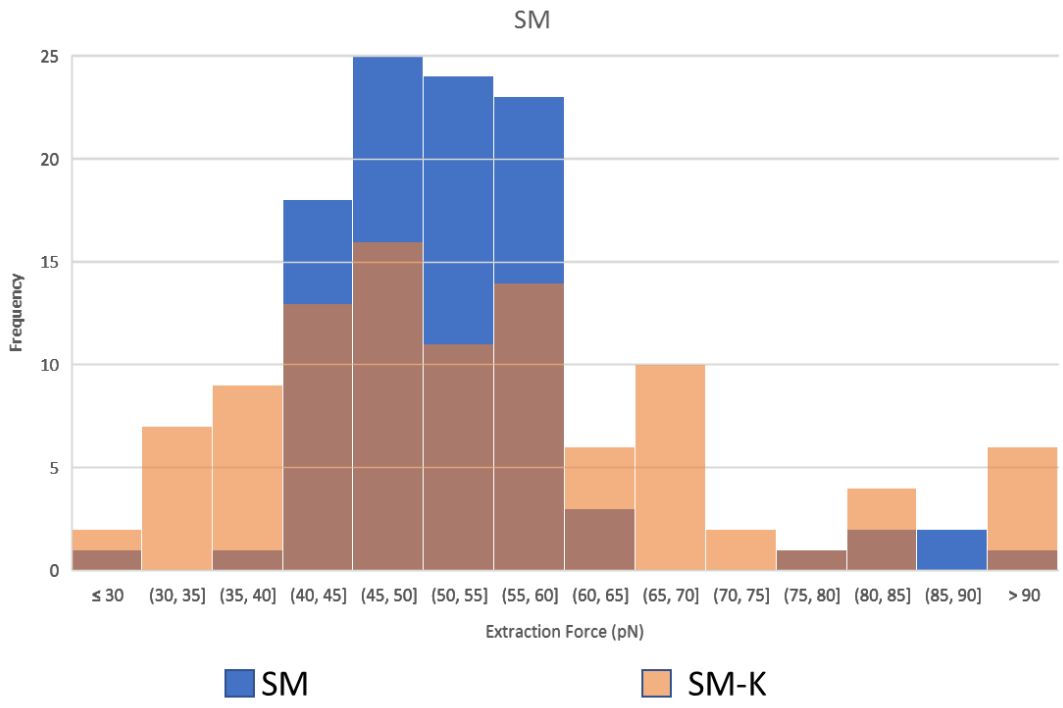

Figure 39: Sphingomyelin containing bilayer cholesterol extraction forces. For these samples there was no clear change in extraction force beyond the variability increasing, evidenced by the broader, spread-out histogram peak of the ketocholesterol containing sample (SM-K, orange, overlap in dark orange) compared to the sample without ketocholesterol (SM, blue).

Table 6: Single thiocholesterol extraction force data for SM bilayer show no clear change in the extraction force required to remove thiocholesterol from the membrane.

		SM	*SM K*
75.00%	quartile	55.65	61.47
50.00%	median	50.97	51.90
25.00%	quartile	46.73	41.88

The SM containing bilayers did not display a decrease in anchoring strength with the inclusion of 7-ketocholesterol – analysis of the data around the main peak shows very little difference in mean extraction force required (Table 6), and there was more variability present in the data (Figure 39); this could indicate that the distribution of 7-keto is not uniform throughout the membrane, or that the lipid composition is varied spatially across the membrane despite no large-scale phase separation appearing in the topography and phase experiments.

This could actually agree with Filippov [32], if there is a connection between the lipid anchoring strength of cholesterol in the membrane and the lateral lipid diffusion characteristics; sphingolipid systems in the L_D phase were largely unaffected by changing cholesterol levels, which could be compared to reducing the effectiveness of cholesterol in membranes by the inclusion of oxysterols. This comparison, however, does not correlate well with the FRAP and force mapping experiments using this explanation – more experiments are required to fully understand these observations, preferably with a higher percentage of cholesterol included in the SM bilayers in order to better mimic lens membranes.

Chapter 5 Conclusions & Future Research Directions

5.1 7-Ketocholesterol: Impact on the lipid membrane and role in disease

This research project has shown that 7-ketocholesterol does have a significant impact on the biophysical properties of lipid bilayer membranes mimicking or extracted from the eye lens. This effect is to Increase the lateral diffusion coefficient, decrease the stiffness of the membrane and, for one of the membranes tested, make it easier to extract single cholesterol molecules from the bilayer.

This result may at first appear anomalous when considering the literature as the lens is known to become stiffer with age and accumulation of damage, but direct comparison of whole tissue behaviour and that of isolated model bilayers would be overly simplistic – there are many factors at work within the whole tissue.

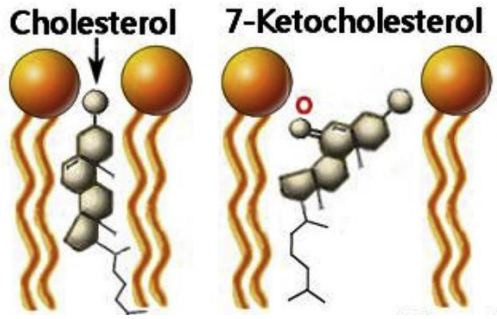

Figure 40: Cholesterol and 7-ketocholesterol positioning in membranes. The additional oxygen in 7-ketocholesterol causes the molecule to tilt within the bilayer, disrupting packing. Image taken from the paper by Brown [134].

Cholesterol is included in membranes as a regulator of fluidity and an agent of order for the lipids of the bilayer, promoting lipids to take the trans rotamer conformation [26]. This effect is diminished in 7-ketocholesterol due to the additional oxygen changing the hydrophobicity and flat shape, causing it to tilt in the bilayer and lose the ability to order surrounding lipids effectively by intercalating (Figure 40).

The ability of the lens to elastically deform relies on all the structural elements of the LFCs, including junctional and channel proteins, cytoskeletal linkages and the membranes themselves working together smoothly – a more fluid bilayer will influence all components of the cell it links to, which could in turn affect the ability of cells to return to their original shape fully once deformed. Disruption of junctional protein arrangement is seen in cataractous lenses [70], and the domain structure of lipids around these junctional proteins would not be as tightly controlled in membranes with significant amounts of 7-ketocholesterol present.

The stiffening of the lens is likely contributed to by other factors than the accumulation of 7-ketocholesterol – for example, the stiffening of the nuclear region of the lens overtaking the cortex which is observed around the age of presbyopia onset [94] is also a time when the entire lipidome of the lens is undergoing a shift in content, with decreasing levels of glycerolipids compared to long-lived sphingolipids [74].

The proteins of the lens are also undergoing changes at this stage of life; large scale binding of crystallin aggregates to LFC membranes is observed during middle age in humans, as levels of soluble crystallin drop and structures including aggregated proteins and lens lipids appear [89]. As there is no appreciable turnover of proteins and lipids in the interior of the lens throughout the entire lifetime this makes sense, as proteins will eventually accumulate damage and lose their functionality as decades pass [85].

The understanding of how 7-ketocholesterol presence affects lens lipid membranes is only one part of the picture, but it is necessary to build on in order to develop a more complete understanding of how different factors influence the eye lens over time.

5.2 Experimental Recommendations

Additional cholesterol extraction experiments on a variety of membrane mimics would be beneficial, as more data is needed to build a representative data set for different lens membranes and quantitatively evaluate the change in average cholesterol anchoring strength.

The next logical step for research would be to create a set of model membranes more closely mimicking different sections of the bovine eye lens (by matching lipid and cholesterol content more closely) and observe the effect of 7-ketocholesterol on these more complicated lipid systems.

When lipid behaviour is better understood in isolation, lens proteins could be incorporated within the structures. Key proteins to include first would be those known to directly associate with membranes in lens, these being AQP0, connexins and BFSP1. Defects in these proteins are known to cause early-onset cataract formation, so full-length proteins and cleavage variants known to be associated with diseases could be studied to observe how their membrane interactions differ. Higher resolution AFM methods could be used to observe the arrangement of proteins within the membranes visually, and combinations of FRAP and dielectric readings could be taken as in Ladha [99] to observe how oxysterols affect the function of membrane pores, channel proteins or aggregation.

The overarching goal is to build up a hierarchical, bottom-up model of healthy eye lens membranes to understand the biophysical properties at each layer of complexity, and then observe how these properties are altered in ageing and disease situations. Comparisons can

be made with native lens membrane extracts from animals of a range of ages, either with proteins extracted or in undisrupted form. The process could also then be applied to the human lens.

It may also be a good idea to look at other oxysterols involved with the eye lens, for example lanosterol-membrane interactions. Lanosterol is an amphipathic molecule which is enriched in the lens and synthesized by lanosterol synthase (LSS), which is also a key reaction of a synthesis pathway for cholesterol. Like BFSP1 mutations, LSS mutations can give rise to congenital cataracts as they can affect the ability of LSS to prevent aggregation of mutant crystallins. It has been suggested that lanosterol could contribute to non-surgical removal of cataracts, but this has not been shown to work for human lenses [122, 135].

5.3 Ongoing Research

Cutting edge research in the area of the eye lens is very much an interdisciplinary area, using physical, chemical and biological data gathered to build up a more complete knowledge of the eye lens in health, disease and ageing. There is a strong focus in the direction of developing medical applications, biological mimic structures and increasingly realistic cell membrane models in simulation. All these areas require observation of behaviours at different length scales and trying to bridge from single molecule scale up to whole tissue.

Stem cell technology is under development and testing, trying to regrow various tissues inside the eye as mentioned previously [136], or outside the body utilising scaffold structures to grow new tissue for later implantation. Scaffold structures are being tested, but are currently more directed at regeneration of other eye tissues, likely due to the unique structural organisation and development of the lens [137, 138].

Biomimic lenses for soft robotics are also being developed (Figure 41) – synchronised soft tuneable lenses have been fabricated that can synchronise focusing with eye movement, taking principles of whole lens structure and transferring to artificial systems that may be developed in time to form better replacements than currently available artificial lenses [139].

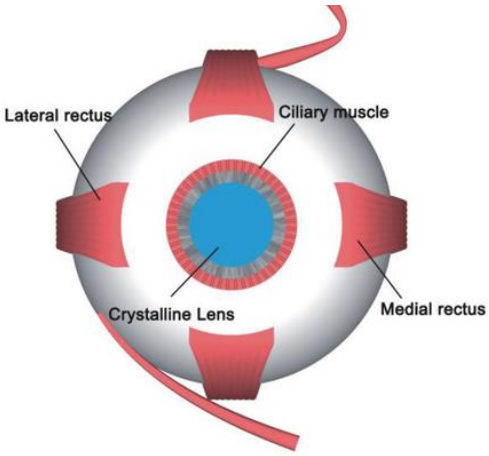

Figure 41: Soft tuneable lens mimic. More sophisticated artificial lenses are being developed for use in soft robots, able to synchronise focus with eye movement. Eventually, smart artificial lens structures like this one, adapted from the paper by Li [139], could be used instead of the current artificial lens replacements.

Computational models of increasingly realistic cell membranes are being developed and used to predict biological phenomena (Figure 42) [140]. To ensure they are accurate depictions of biological behaviours requires comparison with real systems. Models in particular at present are being developed to better match specific tissue membranes, so more information on the wide variety of lipids and other membrane components in biosystems is required.

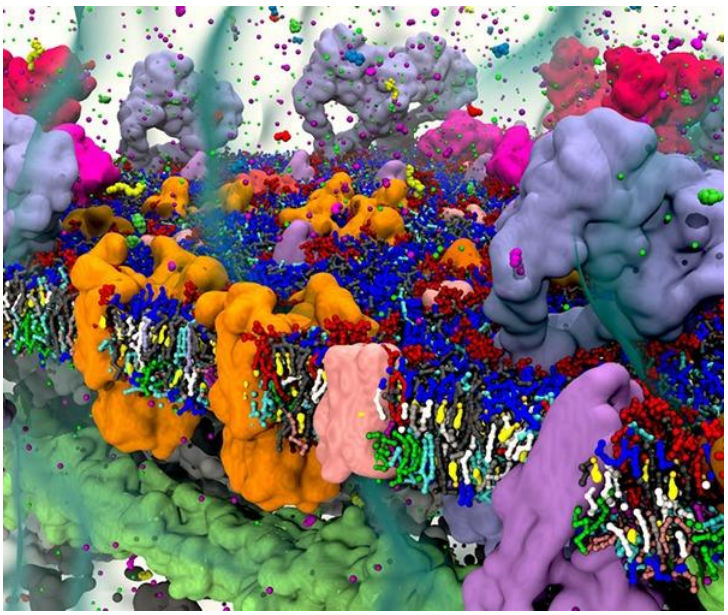

Figure 42: Modelling cell membranes is now possible with increasing levels of complexity, from small scale molecular dynamics simulations to realistic, many component models including large numbers of different lipid and protein types. Figure taken from the paper by Marrink [140].

There is still a requirement to understand observed biological phenomena by understanding the behaviour of individual components on small length scales and in simple models, to back up and inform ongoing research. This work on the behaviour of oxidised sterols on the mechanical properties of lipid bilayer membranes contributes to a greater knowledge base of biophysical behaviours.

Greater understanding of the structural changes to the lens involved in diseases such as cataract and presbyopia may enable new treatment or preventative methods for these conditions to be developed. For example, development of non-surgical intervention to treat cataracts which could be made available in regions where surgical facilities are unreachable is a very desirable goal, or in countries which have an ageing population preventative treatments to halt disease progress before major issues are detectable.

Understanding across different length scales and complexity levels how the lens functions is important for understanding how we age, and how to maintain quality of life into old age. It can be used to inform biologically inspired designs for a variety of applications, and overall increase the understanding of how life works.

Appendices

A) FRAP Imaging Example DOPC: DPPC bilayer

Sample	*Start Frame (t=0 minutes)*	*End Frame (t=10 minutes)*
DOPC: DPPC: Chol	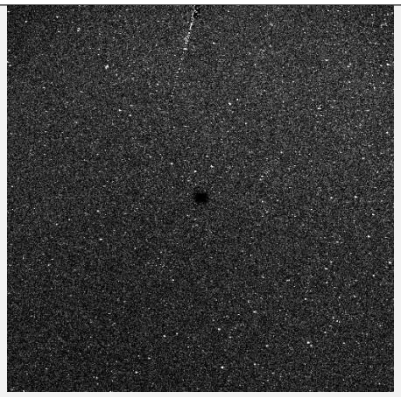	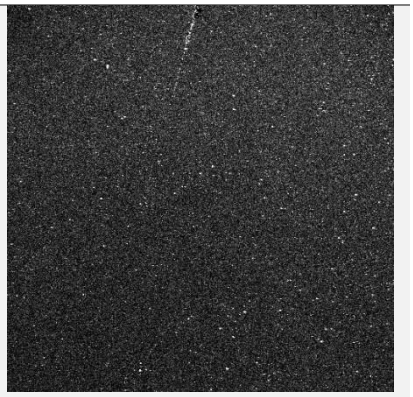

Bibliography

1. Michael-Titus A, Revest P, Shortland P, Michael-Titus A, Revest P, Shortland P (2010) THE VISUAL SYSTEM. Nerv Syst 121–140 . https://doi.org/10.1016/B978-0-7020-3373-5.00007-1
2. Kolb H (1995) Gross Anatomy of the Eye
3. Ott M (2006) Visual accommodation in vertebrates: mechanisms, physiological response and stimuli. J Comp Physiol A 192:97–111 . https://doi.org/10.1007/s00359-005-0049-6
4. Beebe D, Garcia C, Wang X, Rajagopal R, Feldmeier M, Kim JY, Chytil A, Moses H, Ashery-Padan R, Rauchman M (2004) Contributions by members of the TGFbeta superfamily to lens development. Int J Dev Biol 48:845–856 . https://doi.org/10.1387/ijdb.041869db
5. Rujoi M, Jin J, Borchman D, Tang D, Yappert MC (2003) Isolation and lipid characterization of cholesterol-enriched fractions in cortical and nuclear human lens fibers. Invest Ophthalmol Vis Sci 44:1634–42
6. Hockwin O Cataract classification. Doc Ophthalmol 88:263–75
7. Girão H, Mota MC, Ramalho J, Pereira P (1998) Cholesterol oxides accumulate in human cataracts. Exp Eye Res 66:645–652 . https://doi.org/10.1006/exer.1998.0465
8. (2018) WHO | Priority eye diseases. WHO
9. National Eye Institute (2010) Facts About Presbyopia | National Eye Institute. https://nei.nih.gov/health/errors/presbyopia. Accessed 16 Dec 2018
10. Mathias RT, Rae JL (2004) The lens: local transport and global transparency. Exp Eye Res 78:689—698 . https://doi.org/10.1016/j.exer.2003.07.001
11. Bassnett S, Mataic D (1997) Chromatin Degradation in Differentiating Fiber Cells of the Eye Lens. 137:37–49
12. Lo WK, Biswas SK, Brako L, Shiels A, Gu S, Jiang JX (2014) Aquaporin-0 targets interlocking domains to control the integrity and transparency of the eye lens. Investig Ophthalmol Vis Sci 55:1202–1212 . https://doi.org/10.1167/iovs.13-13379
13. Biswas SK, Lee JE, Brako L, Jiang JX, Lo W-K (2010) Gap junctions are selectively associated with interlocking ball-and-sockets but not protrusions in the lens. Mol Vis 16:2328–2341
14. Song S, Landsbury A, Dahm R, Liu Y, Zhang Q, Quinlan RA (2009) Functions of the intermediate filament cytoskeleton in the eye lens. J Clin Invest 119:1837–1848 . https://doi.org/10.1172/JCI38277
15. Borchman D, Delamere NA, McCauley LA, Paterson CA (1989) Studies on the distribution of cholesterol, phospholipid, and protein in the human and bovine lens. Lens Eye Toxic Res 6:703–24
16. Bassnett S, Shi Y, Vrensen GFJM (2011) Biological glass: structural determinants of eye lens transparency. Philos Trans R Soc B Biol Sci 366:1250–1264 . https://doi.org/10.1098/rstb.2010.0302
17. Mathias RT, Kistler J, Donaldson P (2007) The Lens Circulation. J Membr Biol 216:1–16 . https://doi.org/10.1007/s00232-007-9019-y
18. Singer SJ, Nicolson GL (1972) The fluid mosaic model of the structure of cell membranes. Science 175:720–31
19. Nicolson GL (2014) The Fluid - Mosaic Model of Membrane Structure: Still relevant to understanding the structure, function and dynamics of biological membranes after more than 40 years. Biochim Biophys Acta - Biomembr 1838:1451–1466 . https://doi.org/10.1016/j.bbamem.2013.10.019
20. Borchman D, Yappert MC (2010) Lipids and the ocular lens. J Lipid Res 51:2473–2488 . https://doi.org/10.1194/jlr.R004119
21. Borchman D, Yappert MC, Afzal M (2004) Lens lipids and maximum lifespan. Exp Eye Res 79:761–768 . https://doi.org/10.1016/j.exer.2004.04.004

22. Kreps EM, Chirkovskaia E V, Pomazanskaia LF, Avrova NF, Levitina M V [Brain lipids of a mammoth, Elephas primigenius, which died more than 40,000 years ago]. Zh Evol Biokhim Fiziol 15:227–38

23. Li LK, So L, Spector A (1985) Membrane cholesterol and phospholipid in consecutive concentric sections of human lenses. J Lipid Res 26:600–609

24. Kulig W, Cwiklik L, Jurkiewicz P, Rog T, Vattulainen I (2016) Cholesterol oxidation products and their biological importance. Chem Phys Lipids 199:144–160 . https://doi.org/10.1016/j.chemphyslip.2016.03.001

25. World of Molecules (2018) Cholesterol Molecular Struture. In: MediaWiki. https://www.worldofmolecules.com/disease/cholesterol.htm. Accessed 29 Mar 2019

26. Rietveld A, Simons K (1998) The differential miscibility of lipids as the basis for the formation of functional membrane rafts. Biochim Biophys Acta - Rev Biomembr 1376:467–479 . https://doi.org/10.1016/S0304-4157(98)00019-7

27. Chang TY, Telakowski C, Heuvel W V, Alberts AW, Vagelos PR (1977) Isolation and partial characterization of a cholesterol-requiring mutant of Chinese hamster ovary cells. Proc Natl Acad Sci U S A 74:832–6 . https://doi.org/10.1073/PNAS.74.3.832

28. Borchman D, Simon R, Bicknell-Brown E (1982) Variation in the lipid composition of rabbit muscle sarcoplasmic reticulum membrane with muscle type. J Biol Chem 257:14136–9

29. Borchman D, Cenedella RJ, Lamba OP (1996) Role of cholesterol in the structural order of lens membrane lipids. Exp Eye Res 62:191–198 . https://doi.org/10.1006/exer.1996.0023

30. Pike LJ (2006) Rafts defined: a report on the Keystone Symposium on Lipid Rafts and Cell Function. J Lipid Res 47:1597–8 . https://doi.org/10.1194/jlr.E600002-JLR200

31. Goluszko P, Nowicki B (2005) Membrane Cholesterol : a Crucial Molecule Affecting Interactions of Microbial Pathogens with Mammalian Cells Downloaded from http://iai.asm.org/ on January 23 , 2014 by NATIONAL CENTRE FOR BIOLOGICAL SCIENCES Membrane Cholesterol : a Crucial Molecule Affe. 73:7791–7796 . https://doi.org/10.1128/IAI.73.12.7791

32. Filippov A, Orädd G, Lindblom G (2003) The Effect of Cholesterol on the Lateral Diffusion of Phospholipids in Oriented Bilayers. 84:

33. Chatterjee S, Mayor S (2001) The GPI-anchor and protein sorting. Cell Mol Life Sci 58:1969–1987 . https://doi.org/10.1007/PL00000831

34. Subczynski WK, Mainali L, Raguz M, O'Brien WJ (2017) Organization of lipids in fiber-cell plasma membranes of the eye lens. Exp Eye Res 156:79–86 . https://doi.org/10.1016/j.exer.2016.03.004

35. Widomska J, Subczynski WK, Mainali L, Raguz M (2017) Cholesterol Bilayer Domains in the Eye Lens Health: A Review. Cell Biochem Biophys 75:387–398 . https://doi.org/10.1007/s12013-017-0812-7

36. Mainali L, Raguz M, O'Brien WJ, Subczynski WK (2012) Properties of fiber cell plasma membranes isolated from the cortex and nucleus of the porcine eye lens. Exp Eye Res 97:117–129 . https://doi.org/10.1016/j.exer.2012.01.012

37. Alcala J, Lieska N, Maisel H (1975) Protein composition of bovine lens cortical fiber cell membranes. Exp Eye Res 21:581–595 . https://doi.org/10.1016/0014-4835(75)90040-8

38. Wang Z, Schey KL (2015) Proteomic analysis of lipid raft-like detergent-resistant membranes of lens fiber cells. Investig Ophthalmol Vis Sci 56:8349–8360 . https://doi.org/10.1167/iovs.15-18273

39. Zampighi GA, Eskandari S, Hall JE, Zampighi L, Kreman M (2002) Micro-domains of AQP0 in lens equatorial fibers. Exp Eye Res 75:505–19

40. Zampighi G, Simon SA, Robertson JD, McIntosh TJ, Costello MJ (1982) On the structural organization of isolated bovine lens fiber junctions. J Cell Biol 93:175–89

41. Ainsbury EA, Barnard S, Bright S, Dalke C, Jarrin M, Kunze S, Tanner R, Dynlacht JR, Quinlan RA, Graw J, Kadhim M, Hamada N (2016) Ionizing radiation induced cataracts: Recent

biological and mechanistic developments and perspectives for future research. Mutat Res - Rev Mutat Res 770:238–261 . https://doi.org/10.1016/j.mrrev.2016.07.010

42. Andley UP (2007) Crystallins in the eye: Function and pathology. Prog Retin Eye Res 26:78–98 . https://doi.org/10.1016/j.preteyeres.2006.10.003

43. Bloemendal H (1977) The vertebrate eye lens. Science (80-) 197:127 LP – 138 . https://doi.org/10.1126/science.877544

44. Lampi K, Ma Z, Shih M, Shearer T, B Smith J, L Smith D, L David L (1997) Sequence analysis of betaA3, betaB3, and betaA4 crystallins completes the identification of the major proteins in young human lens

45. TROKEL S (1962) The physical basis for transparency of the crystalline lens. Invest Ophthalmol 1:493–501

46. Takemoto L, Sorensen CM (2008) Protein-protein interactions and lens transparency. Exp Eye Res 87:496–501 . https://doi.org/10.1016/j.exer.2008.08.018

47. Kiss AJ, Mirarefi AY, Ramakrishnan S, Zukoski CF, DeVries AL, Cheng C-HC (2004) Cold-stable eye lens crystallins of the Antarctic nototheniid toothfish Dissostichus mawsoni Norman. J Exp Biol 207:4633 LP – 4649

48. Hess JF, Casselman JT, Kong AP, Fitzgerald PG (1998) Primary seq, Secondary structure, gene structure and assembly properties suggests that the lens-specific cytoskeletal protein filensin represents a novel class of intermediate filament protein.pdf. 625–644

49. Wang Z, Schey KL (2017) Identification of a direct Aquaporin-0 binding site in the lens-specific cytoskeletal protein filensin. Exp Eye Res 159:23–29 . https://doi.org/10.1016/j.exer.2017.02.012

50. Agre P (2004) Aquaporin Water Channels (Nobel Lecture). Angew Chemie Int Ed 43:4278–4290 . https://doi.org/10.1002/anie.200460804

51. Varadaraj K, Kumari S, Shiels A, Mathias RT (2005) Regulation of aquaporin water permeability in the lens. Investig Ophthalmol Vis Sci 46:1393–1402 . https://doi.org/10.1167/iovs.04-1217

52. Ball LE, Garland DL, Crouch RK, Schey KL (2004) Post-translational modifications of Aquaporin 0 (AQP0) in the normal human lens: Spatial and temporal occurrence. Biochemistry 43:9856–9865 . https://doi.org/10.1021/bi0496034

53. Kumari SS, Varadaraj K (2014) Aquaporin 0 plays a pivotal role in refractive index gradient development in mammalian eye lens to prevent spherical aberration. Biochem Biophys Res Commun 452:986–991 . https://doi.org/10.1016/j.bbrc.2014.09.032

54. Gonen T, Walz T (2006) The structure of aquaporins. Q Rev Biophys 39:361–396 . https://doi.org/10.1017/S0033583506004458

55. Berry V, Francis P, Kaushal S, Moore A, Bhattacharya S (2000) Missense mutations in MIP underlie autosomal dominant 'polymorphic' and lamellar cataracts linked to 12q. Nat Genet 25:15–17 . https://doi.org/10.1038/75538

56. Sjöhamn J, Hedfalk K (2014) Unraveling aquaporin interaction partners. Biochim Biophys Acta - Gen Subj 1840:1614–1623 . https://doi.org/10.1016/J.BBAGEN.2013.11.012

57. Sindhu Kumari S, Gupta N, Shiels A, Fitzgerald PG, Menon AG, Mathias RT, Varadaraj K (2015) Role of Aquaporin 0 in lens biomechanics. Biochem Biophys Res Commun 462:339–345 . https://doi.org/10.1016/j.bbrc.2015.04.138

58. Chandy G, Zampighi GA, Kreman M, Hall JE (1997) Comparison of the Water Transporting Properties of MIP and AQP1. J Membr Biol 159:29–39 . https://doi.org/10.1007/s002329900266

59. Kistler J, Bullivant S (1980) Lens gap junctions and orthogonal arrays are unrelated. 111:

60. Németh-Cahalan KL, Kalman K, Hall JE (2004) Molecular Basis of pH and Ca 2+ Regulation of Aquaporin Water Permeability . J Gen Physiol 123:573–580 . https://doi.org/10.1085/jgp.200308990

61. Gonen T, Cheng Y, Kistler J, Walz T (2004) Aquaporin-0 membrane junctions form upon proteolytic cleavage. J Mol Biol 342:1337–1345 . https://doi.org/10.1016/j.jmb.2004.07.076

62. Yu XS (2004) Interaction of major intrinsic protein (aquaporin-0) with fiber connexins in lens development. J Cell Sci 117:871–880 . https://doi.org/10.1242/jcs.00945

63. Rose KML, Gourdie RG, Prescott AR, Quinlan RA, Crouch RK, Schey KL (2006) The C terminus of lens aquaporin 0 interacts with the cytoskeletal proteins filensin and CP49. Investig Ophthalmol Vis Sci 47:1562–1570 . https://doi.org/10.1167/iovs.05-1313

64. Wang Z, Schey KL (2011) Aquaporin-0 interacts with the FERM domain of ezrin/radixin/moesin proteins in the ocular lens. Investig Ophthalmol Vis Sci 52:5079–5087 . https://doi.org/10.1167/iovs.10-6998

65. Fan J, Donovan AK, Ledee DR, Zelenka PS, Fariss RN, Chepelinsky AB (2004) γE-crystallin recruitment to the plasma membrane by specific interaction between lens MIP/aquaporin-O and γE-crystallin. Investig Ophthalmol Vis Sci 45:863–871 . https://doi.org/10.1167/iovs.03-0708

66. Kumar NM, Gilula NB (1996) The gap junction communication channel. Cell 84:381–8

67. Söhl G, Willecke K (2004) Gap junctions and the connexin protein family. Cardiovasc Res 62:228–232 . https://doi.org/10.1016/j.cardiores.2003.11.013

68. A. Retamal M (2013) Connexin in Lens Physiology and Cataract Formation. J Clin Exp Ophthalmol 04:1–13 . https://doi.org/10.4172/2155-9570.S1-001

69. Fleschner CR, Cenedella RJ (1991) Lipid-Composition of Lens Plasma-Membrane Fractions Enriched in Fiber Junctions. J Lipid Res 32:45–53

70. Buzhynskyy N, Sens P, Behar-Cohen F, Scheuring S (2011) Eye lens membrane junctional microdomains: a comparison between healthy and pathological cases. New J Phys 13:0–16 . https://doi.org/10.1088/1367-2630/13/8/085016

71. Buzhynskyy N, Hite RK, Walz T, Scheuring S (2007) The supramolecular architecture of junctional microdomains in native lens membranes. EMBO Rep 8:51–55 . https://doi.org/10.1038/sj.embor.7400858

72. Hughes JR, Levchenko VA, Blaksby SJ, Mitchell TW, Williams A, Truscott RJW (2015) No turnover in lens lipids for the entire human lifespan. Elife 2015:1–16 . https://doi.org/10.7554/eLife.06003

73. Huang L, Grami V, Marrero Y, Tang D, Yappert MC, Rasi V, Borchman D (2005) Human lens phospholipid changes with age and cataract. Investig Ophthalmol Vis Sci 46:1682–1689 . https://doi.org/10.1167/iovs.04-1155

74. Hughes JR, Deeley JM, Blanksby SJ, Leisch F, Ellis SR, Truscott RJW, Mitchell TW (2012) Instability of the cellular lipidome with age. Age (Omaha) 34:935–947 . https://doi.org/10.1007/s11357-011-9293-6

75. Witting LA (1965) Lipid peroxidation in vivo. J Am Oil Chem Soc 42:908–13

76. Oborina EM, Yappert MC (2003) Effect of sphingomyelin versus dipalmitoylphosphatidylcholine on the extent of lipid oxidation. Chem Phys Lipids 123:223–232 . https://doi.org/10.1016/S0009-3084(03)00003-3

77. Deeley JM, Hankin JA, Friedrich MG, Murphy RC, Truscott RJW, Mitchell TW, Blanksby SJ (2010) Sphingolipid distribution changes with age in the human lens. J Lipid Res 51:2753–2760 . https://doi.org/10.1194/jlr.M007716

78. Samadi A (2007) Ceramide-induced cell death in lens epithelial cells. Mol Vis 13:1618–26

79. Borchman D, Stimmelmayr R, George JC (2017) Whales, lifespan, phospholipids, and cataracts. J Lipid Res 58:2289–2298 . https://doi.org/10.1194/jlr.M079368

80. Vejux A, Samadi M, Lizard G (2011) Contribution of Cholesterol and Oxysterols in the Physiopathology of Cataract : Implication for the Development of Pharmacological Treatments. 2011: . https://doi.org/10.1155/2011/471947

81. Simons K, Sampaio JL (2011) Membrane Organization and Lipid Rafts. Cold Spring Harb Perspect Biol 3:a004697–a004697 . https://doi.org/10.1101/cshperspect.a004697

82. Lyons MA, Brown AJ (1999) 7-Ketocholesterol. Int J Biochem Cell Biol 31:369–375

83. Vrensen GFJM (2009) Early cortical lens opacities: a short overview. Acta Ophthalmol 87:602–610 . https://doi.org/10.1111/j.1755-3768.2009.01674.x

84. Zarrouk A, Vejux A, Mackrill J, O'Callaghan Y, Hammami M, O'Brien N, Lizard G (2014) Involvement of oxysterols in age-related diseases and ageing processes. Ageing Res Rev 18:148–162 . https://doi.org/10.1016/j.arr.2014.09.006

85. Truscott RJW, Friedrich MG (2016) The etiology of human age-related cataract. Proteins don't last forever. Biochim Biophys Acta - Gen Subj 1860:192–198 . https://doi.org/10.1016/j.bbagen.2015.08.016 Review

86. Barnes S, Quinlan RA (2017) Small molecules, both dietary and endogenous, influence the onset of lens cataracts. Exp Eye Res 156:87–94 . https://doi.org/10.1016/j.exer.2016.03.024

87. Liang JN, Li XY (1991) Interaction and aggregation of lens crystallins. Exp Eye Res 53:61–66 . https://doi.org/10.1016/0014-4835(91)90145-5

88. Tiwary E, Hegde S, Purushotham S, Deivanayagam C, Srivastava O (2015) Interaction of βa3-crystallin with deamidated mutants of αa-and bcrystallins. PLoS One 10: . https://doi.org/10.1371/journal.pone.0144621

89. Friedrich MG, Truscott RJW (2009) Membrane association of proteins in the aging human lens: Profound changes take place in the fifth decade of life. Investig Ophthalmol Vis Sci 50:4786–4793 . https://doi.org/10.1167/iovs.09-3588

90. Truscott RJW, Comte-Walters S, Ablonczy Z, Schwacke JH, Berry Y, Korlimbinis A, Friedrich MG, Schey KL (2011) Tight binding of proteins to membranes from older human cells. Age (Omaha) 33:543–554 . https://doi.org/10.1007/s11357-010-9198-9

91. Gilliland KO, Freel CD, Johnsen S, Craig Fowler W, Costello MJ (2004) Distribution, spherical structure and predicted Mie scattering of multilamellar bodies in human age-related nuclear cataracts. Exp Eye Res 79:563–576 . https://doi.org/10.1016/j.exer.2004.05.017

92. Al-Ghoul KJ, Costello MJ (1993) Morphological Changes in Human Nuclear Cataracts of Late-Onset Diabetics. Exp Eye Res 57:469–486 . https://doi.org/10.1006/exer.1993.1149

93. Shanmugam PM, Barigali A, Kadaskar J, Borgohain S, Mishra DKC, Ramanjulu R, Minija CK (2015) Effect of lanosterol on human cataract nucleus. Indian J Ophthalmol 63:888–890 . https://doi.org/10.4103/0301-4738.176040

94. Wilde GS, Burd HJ, Judge SJ (2012) Shear modulus data for the human lens determined from a spinning lens test. Exp Eye Res 97:36–48 . https://doi.org/10.1016/j.exer.2012.01.011

95. Truscott RJW, Zhu X (2010) Presbyopia and cataract: A question of heat and time. Prog Retin Eye Res 29:487–499 . https://doi.org/10.1016/j.preteyeres.2010.05.002

96. Gerometta R, Candia OA (2016) A decrease in the permeability of aquaporin zero as a possible cause for presbyopia. Med Hypotheses 86:132–134 . https://doi.org/10.1016/j.mehy.2015.11.002

97. Blumenthal D, Goldstien L, Edidin M, Gheber LA (2015) Universal approach to FRAP analysis of arbitrary bleaching patterns. Sci Rep 5:1–9 . https://doi.org/10.1038/srep11655

98. Ishikawa-ankerhold HC, Ankerhold R, Drummen GPC, Biology C, Zeiss C, Gmbh M, Program B, Stress C, Program A (2012) Advanced Fluorescence Microscopy Techniques—FRAP , FLIP , FLAP , FRET and FLIM. 4047–4132 . https://doi.org/10.3390/molecules17044047

99. Ladha S, Mackie AR, Harvey LJ, Clark DC, Lea EJA, Brullemans M, Duclohier H (1996) Lateral Diffusion in Planar Lipid Bilayers : A Fluorescence Recovery after Photobleaching Investigation of Its Modulation by Lipid Composition , Cholesterol , or Alamethicin Content and Divalent Cations. Biophys J 71:1364–1373 . https://doi.org/10.1016/S0006-3495(96)79339-6

100. JACOB R, CENEDELLAH R, MASON R (2000) Determination of Human Eye Lens Membrane Structure By X-Ray Diffraction Analysis. RigakuCom 17:

101. Ma L, Cai Y, Li Y, Jiao J, Wu Z, O'Shaughnessy B, De Camilli P, Karatekin E, Zhang Y (2017) Single-molecule force spectroscopy of protein-membrane interactions. Elife 6:e30493 .

https://doi.org/10.7554/eLife.30493

102. Neuman KKC, Nagy A (2008) Single-molecule force spectroscopy: optical tweezers, magnetic tweezers and atomic force microscopy. Nat Methods 5:491–505 . https://doi.org/10.1038/nmeth.1218.Single-molecule

103. Lebel P, Basu A, Oberstrass FC, Tretter EM, Bryant Z (2014) Gold rotor bead tracking for high-speed measurements of DNA twist, torque and extension. Nat Methods 11:456–462 . https://doi.org/10.1038/nmeth.2854

104. Whited AM, Park PS-H (2014) Atomic force microscopy: A multifaceted tool to study membrane proteins and their interactions with ligands. Biochim Biophys Acta - Biomembr 1838:56–68 . https://doi.org/10.1016/j.bbamem.2013.04.011

105. Haase K, Pelling AE (2015) Investigating cell mechanics with atomic force microscopy. J R Soc Interface 12:20140970–20140970 . https://doi.org/10.1098/rsif.2014.0970

106. Stetter FWS, Cwiklik L, Jungwirth P, Hugel T (2014) Article Single Lipid Extraction : The Anchoring Strength of Cholesterol in Liquid- Ordered and Liquid-Disordered Phases. Biophysj 107:1167–1175 . https://doi.org/10.1016/j.bpj.2014.07.018

107. Ricci M, Quinlan RA, Voïtchovsky K (2017) Sub-nanometre mapping of the aquaporin–water interface using multifrequency atomic force microscopy. Soft Matter 13:187–195 . https://doi.org/10.1039/C6SM00751A

108. Hell SW (2009) Microscopy and its focal switch. Nat Methods 6:24–32 . https://doi.org/10.1038/nmeth.1291

109. Philip J, Carlsson K (2004) 3D image deconvolution in light microscopy : theory and practice. 538–545

110. Patterson G, Davidson M, Manley S, Lippincott-Schwartz J (2010) Superresolution Imaging using Single-Molecule Localization. Annu Rev Phys Chem 61:345–367 . https://doi.org/10.1146/annurev.physchem.012809.103444

111. Rosten E, Jones GE, Cox S (2013) ImageJ plug-in for Bayesian analysis of blinking and bleaching. Nat Methods 10:97–98 . https://doi.org/10.1038/nmeth.2342

112. Cox S, Rosten E, Monypenny J, Jovanovic-Talisman T, Burnette DT, Lippincott-Schwartz J, Jones GE, Heintzmann R (2012) Bayesian localization microscopy reveals nanoscale podosome dynamics. Nat Methods 9:195–200 . https://doi.org/10.1038/nmeth.1812

113. Ovesný M, Křížek P, Borkovec J, Švindrych Z, Hagen GM (2014) ThunderSTORM: A comprehensive ImageJ plug-in for PALM and STORM data analysis and super-resolution imaging. Bioinformatics 30:2389–2390 . https://doi.org/10.1093/bioinformatics/btu202

114. Oreopoulos J, Yip CM (2009) Combinatorial microscopy for the study of protein-membrane interactions in supported lipid bilayers: Order parameter measurements by combined polarized TIRFM/AFM. J Struct Biol 168:21–36 . https://doi.org/10.1016/j.jsb.2009.02.011

115. Sezgin E, Schwille P (2012) Model membrane platforms to study protein-membrane interactions. Mol Membr Biol 29:144–154 . https://doi.org/10.3109/09687688.2012.700490

116. Veatch SL, Keller SL (2003) Separation of Liquid Phases in Giant Vesicles of Ternary Mixtures of Phospholipids and Cholesterol. Biophys J 85:3074–3083 . https://doi.org/10.1016/S0006-3495(03)74726-2

117. Kahya N (2010) Protein-protein and protein-lipid interactions in domain-assembly: Lessons from giant unilamellar vesicles. Biochim Biophys Acta - Biomembr 1798:1392–1398 . https://doi.org/10.1016/j.bbamem.2010.02.028

118. Chiantia S, Kahya N, Ries J, Schwille P (2006) Effects of ceramide on liquid-ordered domains investigated by simultaneous AFM and FCS. Biophys J 90:4500–4508 . https://doi.org/10.1529/biophysj.106.081026

119. Ralf P. Richter *,†, Rémi Bérat and, Brisson AR (2006) Formation of Solid-Supported Lipid Bilayers: An Integrated View. https://doi.org/10.1021/LA052687C

120. Wang E, Wang D, Geng A, Seo R, Gong X (2017) Growth of hollow cell spheroids in

microbead templated chambers. Biomaterials 143:57–64 . https://doi.org/10.1016/j.biomaterials.2017.07.031

121. Lin H, Ouyang H, Zhu J, Huang S, Liu Z, Chen S, Cao G, Li G, Signer RAJ, Xu Y, Chung C, Zhang Y, Lin D, Patel S, Wu F, Cai H, Hou J, Wen C, Jafari M, Liu X, Luo L, Zhu J, Qiu A, Hou R, Chen B, Chen J, Granet D, Heichel C, Shang F, Li X, Krawczyk M, Skowronska-Krawczyk D, Wang Y, Shi W, Chen D, Zhong Z, Zhong S, Zhang L, Chen S, Morrison SJ, Maas RL, Zhang K, Liu Y (2016) Lens regeneration using endogenous stem cells with gain of visual function. Nature 531:323–328 . https://doi.org/10.1038/nature17181

122. Daszynski DM, Santhoshkumar P, Phadte AS, Sharma KK, Zhong HA, Lou MF, Kador PF (2019) Failure of Oxysterols Such as Lanosterol to Restore Lens Clarity from Cataracts. Sci Rep 9:1–14 . https://doi.org/10.1038/s41598-019-44676-4

123. Weikel KA, Garber C, Baburins A, Taylor A (2014) Nutritional modulation of cataract. Nutr Rev 72:30–47 . https://doi.org/10.1111/nure.12077

124. Kistler J, Kirkland B, Gilbert K, Bullivant S (1986) Aging of lens fibers. Mapping membrane proteins with monoclonal antibodies. Investig Ophthalmol Vis Sci 27:772–780

125. Miller EJ, Trewby W, Payam AF, Piantanida L, Cafolla C, Voïtchovsky K (2016) Sub-nanometer Resolution Imaging with Amplitude-modulation Atomic Force Microscopy in Liquid Sub-nanometer Resolution Imaging with Amplitude-modulation Atomic Force Microscopy in Liquid. J Vis Exp. https://doi.org/10.3791/54924

126. Cholesterol Sigma Grade, ≥99% | Sigma-Aldrich. https://www.sigmaaldrich.com/catalog/product/sigma/c8667?lang=en&region=GB. Accessed 19 Nov 2019

127. Stetter FWS, Hugel T (2013) The nanomechanical properties of lipid membranes are significantly influenced by the presence of ethanol. Biophys J 104:1049–1055 . https://doi.org/10.1016/j.bpj.2013.01.021

128. Blumenthal D, Goldstien L, Edidin M, Gheber LA (2015) Universal Approach to FRAP Analysis of Arbitrary Bleaching Patterns. Sci Rep 5:11655 . https://doi.org/10.1038/srep11655

129. Guz N, Dokukin M, Kalaparthi V, Sokolov I (2014) If Cell Mechanics Can Be Described by Elastic Modulus: Study of Different Models and Probes Used in Indentation Experiments. Biophys J 107:564–575 . https://doi.org/10.1016/j.bpj.2014.06.033

130. Bruker Corporation Nanomechanical Property Mapping. http://www.nanophys.kth.se/nanophys/facilities/nfl/afm/icon/bruker-help/Content/ForceVolume/Mechanical Property Mapping.htm#LinearizedHertz. Accessed 24 Feb 2019

131. Girão H, Catarino S, Pereira P (2004) 7-Ketocholesterol modulates intercellular communication through gap-junction in bovine lens epithelial cells. Cell Commun Signal 2:1–10 . https://doi.org/10.1186/1478-811X-2-2

132. Mainali L, Raguz M, O'Brien WJ, Subczynski WK (2013) Properties of membranes derived from the total lipids extracted from the human lens cortex and nucleus. Biochim Biophys Acta - Biomembr 1828:1432–1440 . https://doi.org/10.1016/j.bbamem.2013.02.006

133. Schillers H, Rianna C, Schäpe J, Luque T, Doschke H, Wälte M, Uriarte JJ, Campillo N, Michanetzis GPA, Bobrowska J, Dumitru A, Herruzo ET, Bovio S, Parot P, Galluzzi M, Podestà A, Puricelli L, Scheuring S, Missirlis Y, Garcia R, Odorico M, Teulon JM, Lafont F, Lekka M, Rico F, Rigato A, Pellequer JL, Oberleithner H, Navajas D, Radmacher M (2017) Standardized Nanomechanical Atomic Force Microscopy Procedure (SNAP) for Measuring Soft and Biological Samples. Sci Rep 7:1–9 . https://doi.org/10.1038/s41598-017-05383-0

134. Brown RB (2019) Phospholipid packing defects and oxysterols in atherosclerosis: dietary prevention and the French paradox. Biochimie 167:145–151 . https://doi.org/10.1016/j.biochi.2019.09.020

135. Zhao L, Chen XJ, Zhu J, Xi YB, Yang X, Hu LD, Ouyang H, Patel SH, Jin X, Lin D, Wu F, Flagg K, Cai H, Li G, Cao G, Lin Y, Chen D, Wen C, Chung C, Wang Y, Qiu A, Yeh E, Wang W, Hu X, Grob S, Abagyan R, Su Z, Tjondro HC, Zhao XJ, Luo H, Hou R, P. Perry JJ, Gao W, Kozak

I, Granet D, Li Y, Sun X, Wang J, Zhang L, Liu Y, Yan Y Bin, Zhang K (2015) Lanosterol reverses protein aggregation in cataracts. Nature 523:607–611 . https://doi.org/10.1038/nature14650

136. Lin H, Ouyang H, Zhu J, Huang S, Liu Z, Chen S, Cao G, Li G, Signer RAJ, Xu Y, Chung C, Zhang Y, Lin D, Patel S, Wu F, Cai H, Hou J, Wen C, Jafari M, Liu X, Luo L, Zhu J, Qiu A, Hou R, Chen B, Chen J, Granet D, Heichel C, Shang F, Li X, Krawczyk M, Skowronska-Krawczyk D, Wang Y, Shi W, Chen D, Zhong Z, Zhong S, Zhang L, Chen S, Morrison SJ, Maas RL, Zhang K, Liu Y (2016) Lens regeneration using endogenous stem cells with gain of visual function. Nature 531:323–328 . https://doi.org/10.1038/nature17181

137. Mobaraki M, Abbasi R, Vandchali SO, Ghaffari M, Moztarzadeh F, Mozafari M (2019) Corneal repair and regeneration: Current concepts and future directions. Front Bioeng Biotechnol 7:1–20 . https://doi.org/10.3389/fbioe.2019.00135

138. Stern JH, Tian Y, Funderburgh J, Pellegrini G, Zhang K, Goldberg JL, Ali RR, Young M, Xie Y, Temple S (2018) Regenerating Eye Tissues to Preserve and Restore Vision. Cell Stem Cell 22:834–849 . https://doi.org/10.1016/j.stem.2018.05.013

139. Li J, Wang Y, Liu L, Xu S, Liu Y, Leng J, Cai S (2019) A Biomimetic Soft Lens Controlled by Electrooculographic Signal. Adv Funct Mater 29:1903762 . https://doi.org/10.1002/adfm.201903762

140. Marrink SJ, Corradi V, Souza PCT, Ingólfsson HI, Tieleman DP, Sansom MSP (2019) Computational Modeling of Realistic Cell Membranes. Chem Rev 119:6184–6226 . https://doi.org/10.1021/acs.chemrev.8b00460